Article

# An extension of the MILES library with derived Teff, log g, [Fe/H], and [α/Fe]

García Pérez, A.E., Sánchez-Blázquez, P., Vazdekis, A., Allende Prieto, C., Milone, A de C, Sansom, Anne E, Gorgas, J., Falcón-Barroso, J., Martín Navarro, I. and Cacho, R.



*García Pérez, A.E., Sánchez-Blázquez, P., Vazdekis, A., Allende Prieto, C., Milone, A de C, Sansom, Anne E ORCID: 0000-0002-2782-7388, Gorgas, J., Falcón-Barroso, J., Martín Navarro, I. et al (2021) An extension of the MILES library with derived Teff, log g, [Fe/H], and [α/Fe]. Monthly Notices of the Royal Astronomical Society, 505 (3). pp. 4496-4514. ISSN 0035-8711*

Monthly Notices of the ROYAL ASTRONOMICAL SOCIETY

MNRAS **505,** 4496–4514 (2021) https://doi.org/10.1093/mnras/stab076
Advance Access publication 2021 February 1

# An extension of the MILES library with derived $T_{\rm eff}$, $\log g$, [Fe/H], and [$\alpha$/Fe]

A. E. García Pérez,[1,2]★ P. Sánchez-Blázquez,[3,4]★ A. Vazdekis,[1,2]★ C. Allende Prieto,[1,2] A. de C. Milone,[5] A. E. Sansom,[6] J. Gorgas,[3,4] J. Falcón-Barroso,[1,2] I. Martín Navarro[1,2,7,8] and R. Cacho[3,4]

[1]*Instituto de Astrofísica de Canarias, E-38205 La Laguna, Tenerife, Spain*
[2]*Departamento de Astrofísica, Universidad de La Laguna, E-38206 La Laguna, Tenerife, Spain*
[3]*Departamento de Física de la Tierra y Astrofísica, Universidad Complutense de Madrid, E-28040 Madrid, Spain*
[4]*Instituto de Física de Partículas y del Cosmos, Universidad Complutense de Madrid, E-28040 Madrid, Spain*
[5]*Divisão de Astrofísica, Instituto Nacional de Pesquisas Espaciais, Av. dos Astronautas 1758, São José dos Campos, 12227-010, SP, Brazil*
[6]*Jeremiah Horrocks Institute, School of Physical Sciences and Computing, University of Central Lancashire, Preston PR1 2HE, UK*
[7]*University of California Observatories, Santa Cruz, CA 95064, USA*
[8]*Max-Planck Institut für Astronomie, D-69117 Heidelberg, Germany*

Accepted 2020 December 30. Received 2020 December 4; in original form 2019 March 29

## ABSTRACT

Extragalactic astronomy and stellar astrophysics are intrinsically related. In fact, the determination of important galaxy properties such as stellar masses, star formation histories, or chemical abundances relies on the ability to model their stellar populations. One important ingredient of these models is stellar libraries. Empirical libraries must have a good coverage of $T_{\rm eff}$, [Z/H], and surface gravity, and have these parameters reliably determined. MILES is one of the most widely used empirical libraries. Here, we present an extension of this library with 205 new stars especially selected to cover important regions of the parameter space, including metal-poor stars down to [Fe/H] $\sim -1.0$. We describe the observations and data reductions as well as a new determination of the stellar parameters, including [$\alpha$/Fe] ratio. The new MILES library contains 1070 stars with homogeneous and reliable determination of [Fe/H], $T_{\rm eff}$, $\log g$, and [$\alpha$/Fe] ratio.

**Key words:** stars: abundances – stars: atmospheres – stars: fundamental parameters – galaxies: stellar content.

## 1 INTRODUCTION

Extragalactic astronomy and stellar astrophysics are closely tied. Progress made in understanding stars should directly benefit our ability to model and interpret observations of integrated light from stellar populations. Observations of individual stars in the Milky Way provide detailed information on galactic dynamics and chemistry that complements extragalactic observations. Synergy between these research areas is required to solve some of the most important, but still controversial, questions on galaxy formation and evolution.

Model predictions depend critically on the quality of their ingredients, such as the stellar libraries as illustrated in Vazdekis et al. (2010). Stellar libraries can be empirical, theoretical, or a combination of both (semi-empirical) each of them having pros and cons. Examples of empirical libraries include the Lick IDS (Gorgas et al. 1993; Worthey et al. 1994), Pickles' (Pickles 1998), Jones' (Jones 1999), ELODIE (Prugniel & Soubiran 2001), STELIB (Le Borgne et al. 2003), Indo-US (Valdes et al. 2004), or more recently the SDSS-BOSS library (Kesseli et al. 2017). Other libraries under construction are the MANGA stellar library MaStar (Yan & MaStar Team 2017), or the X-shooter Spectral Library (Chen et al. 2014; Gonneau et al. 2020). Theoretical libraries have been used as well, e.g. BaSeL (Lejeune, Cuisinier & Buser 1997, 1998; Westera et al. 2002), UVBlue (Martins et al. 2005), the libraries of Chavez, Malagnini & Morossi (1997), Bertone et al. (2004), and Coelho et al. (2005), or the semi-empirical collections by Conroy, Graves & van Dokkum (2014) and La Barbera et al. (2017).

A good empirical library should cover a broad range of stellar luminosity classes (dwarfs, giants, supergiants, etc.), spectral types (early to late), and metallicities. The quality in the determination of these stellar parameters is also important. The quality of the spectra is fundamental, including a good calibration of their spectral shape.

MILES (Sánchez-Blázquez et al. 2006) is a reference among the empirical libraries. Beyond stellar population synthesis studies, it has also been applied to the automated analysis of large surveys of Milky Way stars (Xiang et al. 2015). The library included stellar atmospheric parameters based on results from HR studies in the literature (Cenarro et al. 2007, hereafter C07), supplemented with Mg abundance determinations (Milone, Sansom & Sánchez-Blázquez 2011, hereafter MSS11). Despite the efforts in C07 to place all the literature determinations on the same scale, it is very hard to ensure consistency in such a compilation. Independent analyses based on spectral fits are also available, e.g. Prugniel, Vauglin & Koleva (2011), Sharma, Prugniel & Singh (2016). These studies employ the

★ E-mail: agp@iac.es (AEGP); psanchezblazquez@ucm.es (PS-B); vazdekis@iac.es (AV)

**Table 1.** Range in photospheric parameters for the C07 and current characterization. They are different because of the current valid range of the analysis and the extended version of the MILES library.

| Name | $T_{\rm eff}$ | $\log g$ | [Fe/H] |
|---|---|---|---|
| C07 | [2750, 36000] | [−0.2, +5.5] | [−2.9, +1.6] |
| Current | [3756, 27800] | [ +0.05, +4.97] | [−3.1, +1.0] |

ULYSS code (Koleva et al. 2009) and an interpolation code TGM ($T_{\rm eff}$, $\log g$, [Fe/H], $\lambda$), fed with the ELODIE 3.2 library, for estimating the stellar parameters. Finally, MSS11 obtained the magnesium abundance for 76.3 per cent of the stars in the MILES library. High-resolution (HR) spectroscopic measurements of [Mg/Fe] were compiled from several works. The Borkova & Marsakov (2005) values were chosen to define a uniform [Mg/Fe] scale, on to which the majority of the HR measurements were rescaled. These uniform HR measurements included 315 stars (around one-third of MILES). 306 of these stars were employed to define a control sample for calibrating the measurements carried out at the resolution of the MILES spectra (mid-resolution, MR). The MR chemical analysis covered 437 additional stars and was based on spectral synthesis of two Mg features by applying two methods (pseudo-equivalent width and line profile fit). The mean [Mg/Fe] error obtained from the HR measurements was 0.09 dex and the one from the MR measurements was 0.12 dex.

In this work, we present an accurate characterization of the MILES stellar parameters using a similar approach to Allende Prieto (2011) but including five different parameters, $\log g$, [Fe/H], $T_{\rm eff}$, $\alpha$-element abundance, and microturbulent velocity. We apply this method to the original MILES library and to an extension of 205 new stars.

The outline of the manuscript is the following. Section 2 introduces the extension/upgrade of the library. Section 3 describes the spectroscopic analysis to derive the atmospheric parameters. A description of the uncertainties is presented in Section 3.1. We compare the new parameters with previous estimations in Sections 4, 5, and 6. The manuscript ends with discussion of results for the new 193 stars added to the library (Section 7) followed by a summary (Section 8).

## 2 THE MILES LIBRARY

The broad coverage in stellar luminosity and spectral type, chemical composition, and the large number of high-quality and well-characterized spectra makes MILES quite unique among the available stellar libraries. MILES also stands out because of its excellent flux calibration and the correction of interstellar extinction and telluric contamination, as well as its large wavelength coverage at a relatively high spectral resolution for galaxy spectroscopy.

The original library included 985 stellar spectra taken with the Intermediate Dispersion Spectrograph (IDS), at the 2.5-m Isaac Newton telescope, in La Palma, between 2000 and 2001 (Sánchez-Blázquez et al. 2006). The spectra have a spectral resolution of FWHM = 2.5 Å (Falcón-Barroso et al. 2011) and a wavelength coverage of 3500–7429 Å. Table 1 gives the parameter coverage from C07. The majority of the spectra have a high-signal-to-noise ratio S/N $\gtrsim$ 100 per pixel (0.9 Å) at 5200 Å. The library contains 896 field stars and 89 stars in 17 different clusters spanning a wide metallicity range: Alpha Persei, Coma Ber, Hyades, Pleiades, M3, M4, M5, M13, M25, M67, M71, M79, M92, NGC 288, NGC 2420, NGC 6791, and NGC 7789.

### 2.1 An extension to the MILES library

We have extended the MILES library with 205 new stars selected from the PASTEL catalogue (Soubiran et al. 2010) to have relatively low [Mg/Fe] values at $-1 \lesssim$ [Fe/H] $\lesssim 0$, and [Mg/Fe] $> 0.0$ at higher metallicities. We selected stars from Borkova & Marsakov (2005; dwarfs), Thevenin (1998; giants), Alves-Brito et al. (2010), Edvardsson et al. (1993), Bensby et al. (2005; thin and thick disc stars), Stephens & Boesgaard (2002; halo metal-poor dwarfs/subgiants), Mishenina et al. (2004; FGK dwarfs), and Nissen & Schuster (2010). The estimates of the Mg abundances are not on the same scale in all references, but they were only used for the purpose of sample selection.

The observations were carried out in two different runs (A and B) during 2011, using the same instrument (IDS) and telescope (INT) as used in the original MILES library. As in the original library, each star was observed three times; two of them were to cover the blue and red part of the spectra and the third one, obtained with a wide slit oriented along the paralactic angle, was to ensure a proper flux calibration, avoiding chromatic losses due to differential atmospheric refraction. The instrumental set-ups are described in Table 2. The typical signal-to-noise ratio per pixel at 5500 Å is ∼100.

The spectra have been reduced with REDUCME (Cardiel 1999), following the same steps as in the original MILES library. Error spectra were obtained with a parallel treatment of data and error frames through the whole reduction process (the reader is referred to Sánchez-Blázquez et al. 2006 for further details).

The second-order filter used in Run A (52 in total) blocked the signal blueward ∼3900 Å. We adopted for these stars the interpolation algorithm described in Vazdekis et al. (2003, 2015) to replace this spectral range, down to ∼3540 Å. Fig. A1 in Appendix A illustrates this approach. Both versions of the library (with and without interpolation) along with the uncertainties spectrum will be available on http://miles.iac.es/.

The subsections below describe those steps that are specific for the new spectra and therefore not described in the original reference.

#### 2.1.1 *Interstellar reddening*

As in the original MILES library, the spectra were corrected for interstellar reddening using the Galactic extinction curve of Fizpatrick (1999) with $R_V = 3.1$. We followed the same procedure as used in Sánchez-Blázquez et al. (2006) to correct those stars with unknown reddening. These authors calculated a fitting function that predicts the intrinsic colour (reddening free) of a star for a set of $T_{\rm eff}$ and [Fe/H]. This calibration used b4500-b6400 synthetic colour[1] measured on the (reddening corrected) stars with known $E(B-V)$ from the literature[2] with an rms dispersion of 0.013 mag. We calculated again this fitting function using the (reddening corrected) 985 spectra from MILES as shown in Fig. 1.

Because the determination of the stellar parameters depends on the continuum shape, we had to follow an iterative procedure: (1) we first calculated the reddening using the fitting function with the stellar parameters from the literature; (2) we used the reddened corrected

[1]See Sánchez-Blázquez et al. (2006) for details about the colour choice.
[2]References were Savage et al. (1985), Friedemann (1992), Silva & Cornell (1992), Gorgas et al. (1993), Carney et al. (1994), Snow et al. (1994), Alonso, Arribas & Martíinez–Roger (1996), Dyck et al. (1996), Harris (1996), Schuster et al. (1996), Twarog, Ashman & Anthony-Twarog (1997), Taylor (1999), Beers et al. (1999), Dias et al. (2002), Stetson, Bruntt & Grundahl (2003), and V. Vansevicius (private communication).

**Table 2.** Instrumental configurations for the three different observational settings and two runs. Note that the filter applied for excluding second-order contamination was different in the two observing runs (see text for details).

| | Grating | Detector | Dispersion | Width (arcsec) | Coverage | Filter |
|---|---|---|---|---|---|---|
| Red | R632V | EEV10 | 0.90 Å per pixel | 0.7 | 3500–5500 Å | |
| Blue | R632V | EEV10 | 0.90 Å per pixel | 0.7 | 5450–7500 Å | None |
| Wide (A) | R300V | EEV10 | 1.86 Å per pixel | 6.0 | 3350–7500 Å | GG385 |
| Wide (B) | R300V | EEV10 | 1.86 Å per pixel | 6.0 | 3350–7500 Å | WG360 |

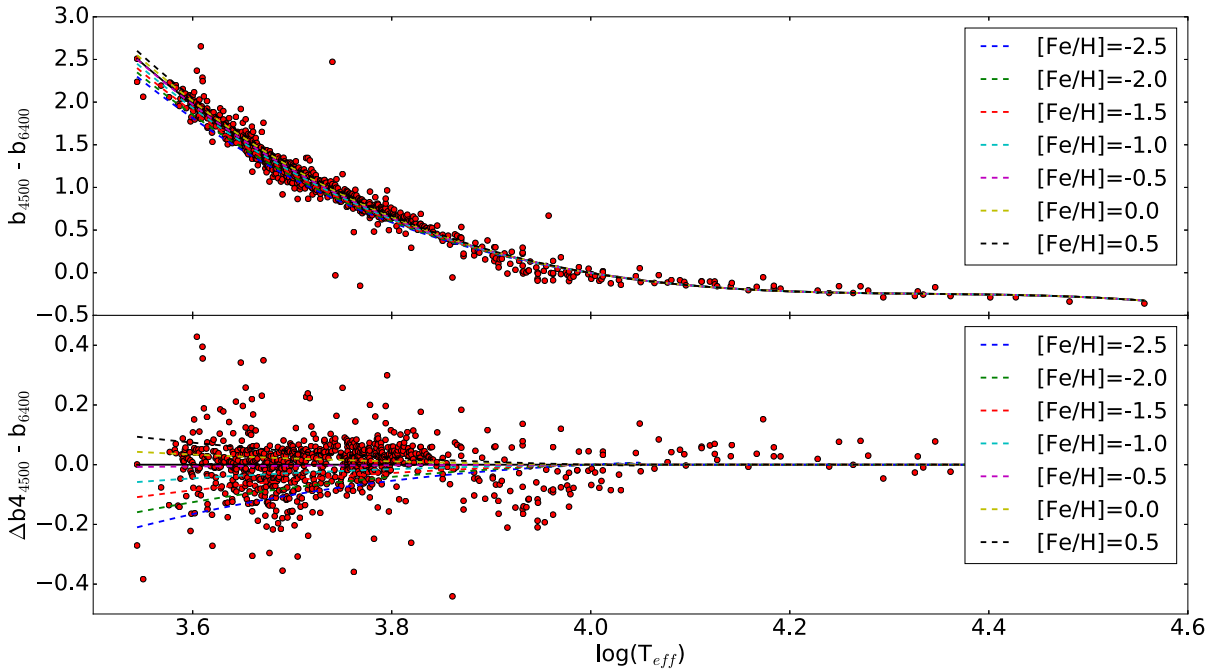


**Figure 1.** Fitting functions used to estimate ($b4500 - b6400$) as a function of $T_{\rm eff}$. Upper panel shows different relations depending on the metallicity. Lower panel shows the residuals from the relation with [Fe/H] = 0.0.

spectra to calculate a first set of stellar parameters; (3) we introduced these new parameters in the fitting function to obtain a new value of the $E(B-V)$; and (4) we used this value to obtain new reddening corrected spectra. We repeated this procedure until the difference in colour excess was less than 0.005 mag.

### 2.1.2 *Spectral resolution*

The spectral resolution of the extension stars was estimated adopting the same methodology employed in Falcón-Barroso et al. (2011) for the original MILES library, with the minor difference that the PHOENIX models (Husser et al. 2013) were used as templates. Results shown in Fig. 2 are based on measurements made only on stars whose best-fitting solutions have residuals below 5 per cent for all the wavelength bins (i.e. 92 per cent of the fits). Bad fits mostly affected the bluest wavelength bins causing a marginal increase in the overall measured full width at half-maximum (FWHM). The figure shows the variation of spectral resolution with wavelength for the newly observed stars, with a typical FWHM estimate of 2.76 Å. The upgraded version of the MILES library is provided at this spectral resolution. For this purpose, the original MILES stellar spectra, with FWHM = 2.50 Å, were degraded to a constant FWHM of 2.76 Å, thus providing a homogeneous data set.

## 2.2 Accuracy of flux calibration via comparison with observed photometry

Fig. 3 compares the $(B-V)$ colour synthesized from MILES spectra before interestellar reddening correction, with the compilation of the Laussanne database/footnotehttp://obswww.unige.ch/gcpd/gcpd.html (Mermilliod, Mermilliod & Hauck 1997).

We estimate the mean offset assuming that the deviations can be fitted with a Cauchy distribution and using a Markov chain Monte Carlo (MCMC) procedure. This procedure takes into account the individual photometric uncertainties and allows for the inclusion of a possible additional uncertainty. The mean offset, 0.001 mag, with a 95 per cent highest density interval (HDI) spanning from 0.000 to 0.002, indicates that $B-V$ are slightly bluer than those in Mermilliod.

It must be noted that stars with the largest discrepancies between the synthetic and observed photometry are, in almost all cases, supergiant stars, in particular classic cepheids, whose inherent colour variations can explain the observed offsets.

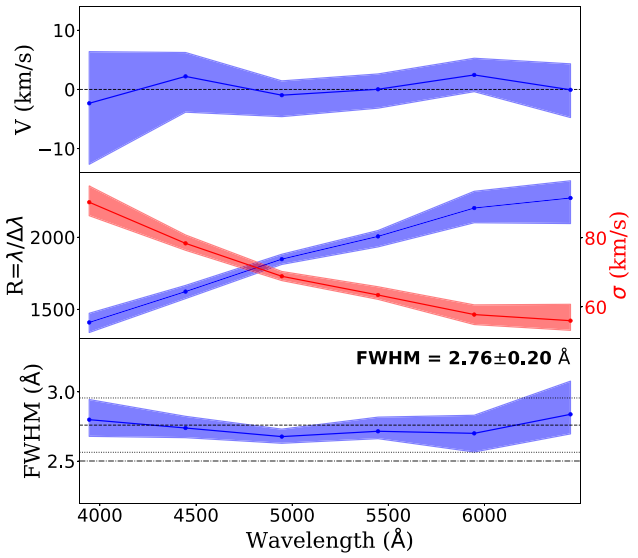


**Figure 2.** Mean radial velocity (top panel), spectral resolution (medium panel; also in terms of velocity dispersion in red), and FWHM (bottom panel) as a function of wavelength for the stars in the MILES extension. Shaded areas indicate $1\sigma$ dispersion and the dashed line in the bottom panel shows the mean spectral resolution of the original library.

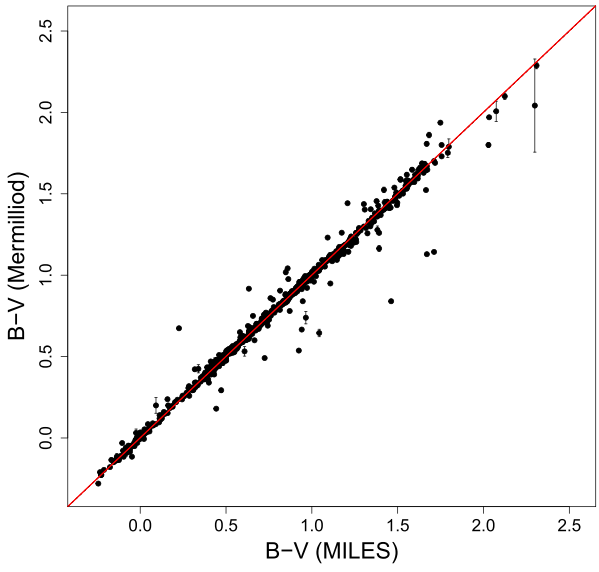


**Figure 3.** Comparison of $(B-V)$ from the Mermilliod catalogue and that measured on the MILES spectra, both uncorrected for extinction. The black dashed line indicates the 1:1 relation. The red line, which almost coincides with the 1:1 relation, shows the mean constant offset (0.001 mag) between both sources of photometry.

It is worth to note that this approach allows us to check the flux calibration accuracy achieved in the spectral region covered by the $B-V$ colour. Checking the remaining spectral portions, blueward $B$ and redward $V$ is in principle possible. Unfortunately, the $U$ and $R$ bands are not fully covered by the MILES spectral range. Redefining the wings of these filters to match the MILES range wavelength ends is a possibility to further this study. However, in doing so, we introduce uncertainties that do not help to constrain the flux calibration accuracy. Moreover, photometric libraries are needed for this calibration, as other spectral libraries might be affected from flux calibration issues.

## 3 SPECTROSCOPIC ANALYSIS

We derive $T_{\rm eff}$ $\log g$, [Fe/H], [$\alpha$/Fe], and $\xi_{\rm t}$ directly from the MILES spectra using an automated spectral synthesis analysis. We generate synthetic spectra with the ASS$\epsilon$T (Koesterke, Allende Prieto & Lambert 2008; Koesterke 2009) code on a grid of ATLAS9 model atmospheres (plane-parallel geometry, Local Thermodynamic Equilibrium (LTE) conditions, and a distribution of opacities; Mészáros et al. 2012). We adopted solar abundances from Asplund, Grevesse & Sauval (2005) and allow for variations of $\alpha$-elements (O, Ne, Mg, Si, S, Ca, and Ti). The line list was built with atomic and molecular data downloaded from the Kurucz website.[3] This list included data for the following molecules: $H_2$, CH, $C_2$, CN, CO, NH, OH, MgH, SiH, and SiO. Bands of TiO from Schwenke (1998) were included only for models with $T_{\rm eff} < 5750$ K. Partition functions were adopted from Irwin (1981 and updates). The synthetic spectra were convolved with a Gaussian kernel to account for instrumental broadening, with FWHM $= 2.5$ Å (2.8 Å for the extension), and resampled to a linear step of $\Delta\lambda = 0.9$ Å.

The synthetic spectra were grouped in five different grids according to their $T_{\rm eff}$. The range of free parameters in the FERRE library used for each group is listed in Table 3. The lower limit in gravity was imposed by the available range of model atmospheres at different temperatures. More details about these libraries can be found in Allende Prieto et al. (2018).

Each individual spectrum, either observational or theoretical, was scaled by its average flux (measured in the whole spectral range) before comparing them. Flux error spectra for the MILES stars, which were obtained by propagating the errors during data reduction as described in Section 2.1, were considered in the fitting process. The optimization was carried out with version 4.7.2 of FERRE[4] (Allende Prieto et al. 2006) using the Nelder–Mead algorithm (Nelder & Mead 1965). This algorithm compares the $\chi^2$ at the test points of a simplex (a triangle in two dimensions), and proceeds reflecting and stretching the simplex to search for the minimum $\chi^2$. The search stops when the convergence criterion is satisfied, i.e. when a standard deviation below $10^{-4}$ for the $\chi^2$ values evaluated at the test points is reached. Other available algorithms were tested but no significant improvement was observed. Quadratic Bézier curves were employed for interpolating in grids of synthetic spectra during the search (see Mészáros & Allende Prieto 2013 for a discussion of interpolation uncertainties). The basis of the method, applied to infrared (IR) spectra, is explained in more detail in García Pérez et al. (2016).

Solutions coming from the multiple FERRE libraries were compared, and that providing the minimum $\chi^2$ was adopted, discarding solutions with parameters or abundances near or on the limits of the associated spectral library. A minimum distance to the grid edge of 10 per cent of the step size was enforced, to avoid issues related to inaccuracies in the interpolations near the limits.

In those cases where all individual solutions are close to grid edges, the solution from the coolest spectral library was adopted. A second analysis was performed for spectra whose final $\log g$ estimates lie exactly at the edge of the spectral library, or if $\log \xi_{\rm t}$ lies in the lower edge. In this additional analysis, the parameter ($\log g$ or $\log \xi_{\rm t}$, depending on the case) is fixed to the value corresponding to the

[3] http://kurucz.harvard.edu/linelists.html
[4] https://github.com/callendeprieto/ferre

**Table 3.** List of synthetic spectral libraries along with their parameter ranges and step sizes.

| Name | $T_{\rm eff}$ (K) | $\log g$ (cgs) | [Fe/H] | [$\alpha$/Fe] | $\log \xi_{\rm t}$ $\log {\rm km\,s^{-1}}$ |
|---|---|---|---|---|---|
| | | | Range; step | | |
| n_miles1 | (3500, 6000); 250 | (0, 5); 0.5 | (−5.0, +1.0); 0.25 | (−1, +1); 0.25 | (−0.301, +0.903); 0.301 |
| n_miles2 | (5750, 8000); 250 | (1, 5); 0.5 | (−5.0, +1.0); 0.25 | (−1, +1); 0.25 | (−0.301, +0.903); 0.301 |
| n_miles3 | (7000, 12000); 500 | (2, 5); 0.5 | (−5.0, +1.0); 0.25 | (−1, +1); 0.25 | (−0.301, +0.903); 0.301 |
| n_miles4 | (10000, 20000); 1000 | (3, 5); 0.5 | (−5.0, +1.0); 0.25 | (−1, +1); 0.25 | (−0.301, +0.903); 0.301 |
| n_miles5 | (20000, 30000); 1000 | (4, 5); 0.5 | (−5.0, +1.0); 0.25 | (−1, +1); 0.25 | (−0.301, +0.903); 0.301 |

edge, but we add +0.1 (except for the upper edge) and 0 for the $\log g$ and $\log \xi_{\rm t}$, respectively. Note that this shift in the parameter was introduced to avoid the grid-edge problem. To summarize, for the stars facing this problem a second iteration was applied in which a parameter is fixed. This can be traced following the flagging scheme described in Section 3.2.1.

FERRE delivers parameter and abundance uncertainties associated with the fitting procedure and the S/N of the data. The uncertainties are based on the inverse of the curvature matrix (Press, Flannery & Teukolsky 1986). All this is done under the assumption that the likelihood of the data is given by $\chi^2(\mathcal{L} \propto {\rm e}^{-\chi^2/2})$ and synthetic spectra describe the observations well. The elements of the matrix are calculated from partial derivatives of the synthetic spectra divided by the square of the uncertainties in the observed fluxes. Departures from this ideal case will affect the uncertainties of the analysis.

### 3.1 Optimization

The spectral analysis is sensitive to some of the assumed conditions. For that reason, it was necessary to adjust the methodology for different stellar spectral types and different sets of observations. The optimal choice for continuum normalization, wavelength range, or set of fitting parameters, was stellar temperature dependent. Analysis of the coolest ($\lesssim$4000 K) and hottest stars ($\gtrsim$12 000 K) turned out to be the most challenging, showing a larger disagreement with the literature. Therefore, the study of very cool stars (<3750 K) was postponed for a future paper (our models cover down to 3500 K). Discrepancies with the literature for the very cool stars may be partly associated with molecular bands and their inaccurate spectral modelling (e.g. inaccurate oscillator strength values, and/or atmospheric structures).

The continuum shape contains very valuable information, in particular on the stellar effective temperature, and we have avoided continuum normalization procedures that eliminate this information. Both observations and synthetic spectra were scaled by their mean values, preserving the continuum shape. This has the disadvantage that the fitting procedure may be affected by uncertainties in flux calibration and reddening extinction corrections, but there are only a few spectra compromised by that choice, and they are readily recognized from the poorly fitted continuum slopes.

We tested alternative normalization schemes for comparison. A median filter with a width of 10 pixels was employed for removing the continuum shape. This led to the following median differences with our previous parameters (*rescaling* − *medianfilter*): +72 K ($T_{\rm eff}$), +0.26 dex ($\log g$), −0.04 dex ([Fe/H]), and +0.04 ([$\alpha$/Fe]). Note that rather than focusing on the outliers, the ultimate aim of this comparison is to provide an assessment on the possible systematic affecting the whole sample. The final normalization choice (to retain the stellar continuum) delivered a better agreement with literature predictions, in spite of uncertainties associated with the flux calibration and reddening extinction.

The spectral fitting process required masking of certain spectral regions:

(i) **Masking in the blue side.** Only wavelengths redder than 4400 Å were considered for stars with $T_{\rm eff} \lesssim 5800$ K. Indeed, unexpectedly high metallicities, accompanied by uncommon positions in the Hertzsprung–Russell (H–R) diagram, appear when these blue regions were unmasked. These regions are more affected by uncertainties in modelling molecular bands, caused by effects such as surface temperature inhomogeneities, non-LTE line formation, and non-solar scaled carbon abundances affecting the CN features. These aspects are not included in the current analysis. For hotter stars, only the wavelengths blueward 3900 Å were discarded in the fits for the stars in the MILES extension due to the lack of signal as discussed in Section 2.1. Note that no blue masking was applied to the hotter stars in the original MILES sample.

(ii) **Masking in the red side.** Wavelengths redward 6800 Å were not considered for the fits of all the stars either from the original or the extended samples. This is due to the use of filters to avoid cross-order contamination affecting the red spectral end.

The masking of the blue region (4400 masking) is necessary for handling systematic differences between our models and nature, but the removal of information also carries a risk of introducing degeneracies or increasing the uncertainties in derived parameters. This risk was evaluated by comparing the results of fitting individual models from our libraries of synthetic spectra, artificially degraded with Gaussian noise to S/N = 100, with and without masking the blue region. The analysis recovered the input parameters well, especially for cool stars. We estimated average uncertainties under 0.01 dex (quantified by a robust dispersion estimator $\sigma_{\rm r}$)[5] (almost zero for $T_{\rm eff}$) for a sample of 1618 spectra with metallicities $> -1.0$ and $T_{\rm eff} = 3750$–11 500 K. These spectra were selected from the synthetic libraries to span the parameter coverage of the MILES library. More uncertain was recovery of the surface gravity, particularly for warm stars (5750 K $< T_{\rm eff} <$ 8000 K). Uncertainties increased threefold when using masking in the blue, 0.006 (unmasked) to 0.019 dex (masked). For avoiding large $\log g$ uncertainties, the final analysis of stars with $T_{\rm eff} > 5800$ K covers the entire spectral range.

The sensitivity of derived parameters to the blue masking was also checked directly on the observations. Analysis of the original MILES stars was not dramatically affected by the introduction of the mask, although systematic offsets were apparent. The largest changes were observed for [$\alpha$/Fe] and $\log g$ with median shifts of −0.31 and +0.15 dex, respectively. Scatter in the distribution of differences

[5] $\sigma_{\rm r}$ is derived measuring the width of the distribution after rejecting 15 per cent of the sample on each side and dividing it by two. This corresponds aproximately to 1$\sigma$ for a Normal distribution).

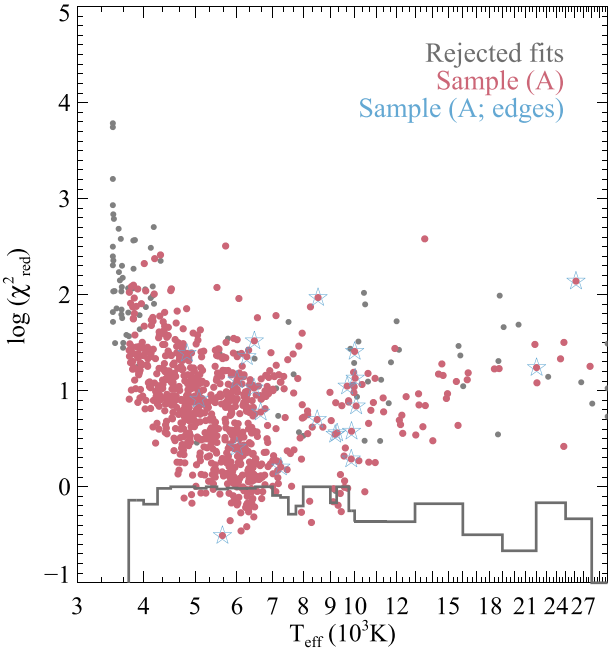


**Figure 4.** log $\chi^2$ red versus $T_{\rm eff}$ for analysis of the field sample of original MILES. Good FERRE spectral fits are shown in red, while the rest are in grey (bad fits or $T_{\rm eff} < 3750$ K). Stars in the grid edges but with good fits appear in blue. The histogram represents the fraction of good stars in temperature bins of 250 K (3000 K for $T_{\rm eff} > 10\,000$ K). For clarity, the histogram is shifted by −1 so that 1 is represented by 0 in the plot.

in log $g$ is also significant, at about 0.2 dex. Stars with the highest sensitivity to blue masking are those with $T_{\rm eff}$ around 7000 K and a special group of metal-rich stars in the range of $T_{\rm eff} = 4000$–5000 K. This special group shows, in the absence of the blue masking, very high parameter estimates in comparison to literature values, with derived metallicity close to +1 and $T_{\rm eff}$ offsets of typically +400 K. The sensitivity for the other stars with $T_{\rm eff} < 7000$ K is more modest.

We also investigated the effect of masking the Na I 5890 doublet, as well as the centre of the Mg II 5170 triplet and H $\alpha$ lines, and found little sensitivity. For the MILES original stars, typical differences with the full analysis are below 20 K ($\Delta T_{\rm eff}$) and 0.1 dex ($\Delta \log g$), or even smaller for the rest of parameters (< 0.05 dex for $\Delta$[Fe/H] and $\Delta[\alpha/{\rm Fe}]$).

The number of free parameters in our analysis varies with spectral type. Unlike for the coolest stars for which five parameters were considered, only two were considered for stars warmer than 10 000 K: $T_{\rm eff}$ and log $g$. The three remaining parameters were kept fixed, assuming $\xi_{\rm t} = 1\,{\rm km\,s^{-1}}$ and solar ratios for [Fe/H] and [$\alpha$/Fe]. This choice was motivated by the fact that spectra are insensitive to variations in metal abundances at the warm temperatures and high ionization level in these atmospheres.

### 3.2 Quality checks

The analysis was applied to all the spectra, but some of them were subsequently rejected after quality assurance, hence the difference with C07 in the coverage range (see Table 1 for the final parameter coverage). The rejected spectra exhibit significant residuals (high $\chi^2$), indicative of poor fits. The final sample selection is based on a visual inspection of the observed spectra and their best-fitting models.

Fig. 4 shows $\chi^2_{\rm red}$ for field stars in the original MILES library. The residuals are a function of effective temperature. The coolest and warmest stars tend to show the largest $\chi^2$ values, which was taken into account in deciding which stars to retain. The reason why $\chi^2$ degrades for lower $T_{\rm eff}$ has to do with the complexity of opacities due to the increase of line absorption, atomic, and especially molecular. There are different causes of rejection, e.g. the presence of low-frequency wiggles in the spectra, different continuum slopes in the blue and red spectral ranges, unmatched molecular bands, or too-low temperatures (<3750 K). The histogram in Fig. 4 shows the fraction of accepted stars as a function of effective temperature (values have been shifted by −1 for clarity). The analysis is fairly successful, with acceptance fractions of >80–90per cent, especially in the regime of 3750 K < $T_{\rm eff}$ < 7000 K. Poor residuals are not the only cause of rejection, and proximity to the grid edges is also an issue in some cases.

#### 3.2.1 *Flagging scheme*

The parameter estimates are flagged according to the quality of the spectral fits. The following flags are used:

(i) 0: Bad fit.
(ii) 1: Good fit.
(iii) 2: Good fit although close to a model grid edge.
(iv) 3: Good fit despite model edge proximity to all relevant model libraries.
(v) 4: Bad fit and model edge proximity.
(vi) 5: Bad fit and edge proximity for all relevant model libraries.

The same scheme applies if a second analysis is performed, which is the case for all the stars with an edge proximity parameter estimate. In this case, the flag digit is duplicated (e.g. 22 stands for a good fit plus an edge proximity in the second analysis). The criteria adopted for raising the grid edge proximity flag is 0.01 dex (0.02 dex) and 50 K (250 K) at the lower (upper) side of the grid, with each free parameter inspected individually.

## 4 NEW STELLAR ATMOSPHERIC PARAMETERS

This work presents new stellar parameter determinations of the original MILES library. Among other features, this study is characterized by its homogeneity and, unlike in other studies, here the stellar parameters including overall $\alpha$-element abundance are derived simultaneously. The quality of the new set of parameters is discussed here.

A total of 984 stars were analysed, 895 field targets and 89 stars in clusters, 46 of which (42 field, 4 in clusters) ended up being cooler than our imposed lowest limit of 3750 K. Our final sample after removing the stars with very cool $T_{\rm eff}$ and/or bad fits includes 877 stars (804 field, sample A; 73 in clusters, sample A'), 23 of which lie near the grid-edges (22 field; 1 in clusters). Regarding the bad fits, there is a total of 61 stars in the temperature range of interest, 30 of which are affected by the grid-edge problem (28 field; 2 in clusters). A list of the different subsamples presented in this study, along with a brief description, is given in Table 4.

Most field and cluster stars enjoy good-quality spectral fits, especially at temperatures where the models have been widely tested (4200 K–7000 K) in the literature, as illustrated in Figs 5 and 6. Typically, the residuals are under a few per cent, especially for warmer stars. The coolest or lowest S/N spectra show slightly larger residuals of ∼10 per cent, in particular in the blue part of the spectrum, where, curiously, the residuals show the largest departures

**Table 4.** A list and description of different MILES samples and subsamples.

| Sample | Characteristics | Size |
|---|---|---|
| A (A') | FINAL: good FERRE fits; $T_{\rm eff} > 3750$ K | 804 (73) |
| B (B') | Subsample fully characterized in C07 (all three parameters) | 772 (73) |
| C (C') | Subsample fully characterized in MSS11 (Mg) | 647 (57) |
| D | Subsample in common with ELODIE | 162 |
| E | Subsample in common with ELODIE and MSS11 | 159 |
| I | Subsample in common with APOGEE | 45 |
| J | Extra sample | 193 |

*Note.* Cluster information is given between parentheses.

from the flux uncertainties (they were expected to be similar). Overall, residuals tend to be a few times larger than the assumed flux errors, which may be indicative of underestimated observational uncertainties, but also inaccurate spectral modelling. Despite the goodness of the fits, some small structures are present in the residuals (see the green curves in Figs 5 and 6), e.g. low-frequency features possibly associated with uncertainties in the flux calibration, or the presence of a depression in the red. Interestingly, the Na I 5890 doublet, the Mg II 5170, and H$\alpha$ lines present large systematic residuals. The formation of the latter lines happens quite high in the photosphere, where departures from LTE are more prominent, and the role of inelastic hydrogen collisions becomes more prominent, making the modelling of these lines uncertain (e.g. Allard et al. 2008; Barklem 2016; Amarsi et al. 2018).

Finally, the FERRE [$\alpha$/Fe] values were found to be significantly lower than expected. Negative values are obtained around solar metallicity, where near-zero values are expected. In fact, the [$\alpha$/Fe] results for solar-like targets are not exactly zero when masking the wavelengths below 4400 Å. But this is not only the result of the applied masking, as other factors cannot be discarded such as systematics in the model atmospheres, line formation physics, or input atomic and molecular lines. Note also that the continnum was taken into account in the analysis and therefore the possibility of differences in the spectral shape of the models and data cannot be discarded, as well as reddening and flux calibration residuals in the latter. To fix this problem and calibrate the zero-point, the [$\alpha$/Fe] values were rescaled using the analysis of the stars HD 10307 and HD 95128, classified as solar analogues in Soubiran & Triaud (2004; HD 95128 also in Mahdi et al. 2016). The $\alpha$-content found for these stars is [$\alpha$/Fe] $\sim -0.20$ (see Table 5), which indeed is too low, and thus our final values of [$\alpha$/Fe] at $T_{\rm eff} < 5800$ are the result of applying that offset to the original determinations.

### 4.1 Field stars

Fig. 7 presents the MILES H–R diagram accompanied by the map of the $\alpha$-content (only field stars with good fits are presented), based for the first time on a homogeneous spectral analysis. The new estimates (red symbols) are given in Table 6, also available online. The results cover the main sequence up to the red giant branch and they show the typical Milky Way pattern for $\alpha$-elements – i.e. higher [$\alpha$/Fe] at lower metallicities and the 'knee' at [Fe/H] $\sim -1$ – in good agreement with stellar and Galactic evolution expectations.

An interesting feature of this new parameter characterization is the significant spread found for the [$\alpha$/Fe] content at low or high metallicity. The spread ($\sigma_{\rm r} \sim 0.2$–$0.3$) is slightly larger than the typical uncertainty in the parameter ($\sigma_{\rm r} \sim 0.1$–$0.2$ dex; see Section 5.3). Stars in the lower [$\alpha$/Fe]-envelope tend to lie in the warm side of the H–R diagram ($\sim$6000 K), thus their [$\alpha$/Fe] content are prone to be more uncertain. Indeed, in some cases, their internal uncertainties are larger than for the averaged sample. Other features of interest are the extremely metal-rich stars, close to the upper limit of the employed grids of synthetic spectra (+1.00).

Internal uncertainties of the parameters and abundance for dwarfs returned by FERRE are about 0.05 dex for the surface gravity and abundances ([Fe/H] and [$\alpha$/Fe]), and even smaller for giant stars. The internal uncertainties for the effective temperatures are also fairly small, typically under 10 K (30 K for hotter stars). These uncertainties reflect the sensitivity of the $\chi^2$ curvature to changes in the parameters taking into account random uncertainties in the stellar fluxes. Nevertheless, it is expected that these uncertainties are underestimated as systematic errors are unaccounted for in their evaluation.

## 5 COMPARISON TO MILES PREVIOUS STELLAR PARAMETERS

There are different characterizations for the stellar parameters of the MILES library, and a comparison is useful for contextualizing the new results. In addition, such comparison is also useful for assessing potential differences in the predictions obtained with stellar population synthesis models when these codes are fed with the new stellar parameters.

The literature parameters compiled in C07 include a homogenization process, which takes as a reference system the ELODIE study of Soubiran, Katz & Cayrel (1998). The $T_{\rm eff}$ range considered here is 3750–10 000 K as metallicities and $\alpha$-content are not analysed outside that range. Not all of the field stars have estimates for all three main parameters in C07 and some are missing from the Mg abundances reported in MSS11. Therefore, the current analysis provides a full characterization (included $\alpha$-content) for 103 field and 16 cluster extra stars. The new parameter estimates are shown in red in Fig. 7, while those of C07 and MSS11 are plotted in grey. These diagrams illustrate the main atmospheric parameters coverage of the MILES library and allow a quick assessment of the differences between these two sets of estimates. A more detailed comparison is developed in the following subsections. Overall, the new characterization for field stars agrees well with C07 + MSS11, but the agreement level varies with effective temperature. Similar conclusions are obtained if the comparison is restricted to stars in common with those that serve as a reference in C07 (ELODIE; Soubiran et al. 1998).

### 5.1 Cool versus hot stars

Fig. 8 shows the differences with C07 + MSS11 in terms of photospheric parameter offsets as a function of $T_{\rm eff}$ (left). Also shown are the corresponding offsets histograms (right). A clear distinction between the cooler and warmer stars is observed, making it necessary to subdivide the field sample. A total of 772 (subsample B; C07) and 647 (subsample C; MSS11) field stars were compared between the two analyses. Only stars with all the three main photospheric parameters reported in C07 are considered (full characterization in C07). The cluster sample consists of 73 fully characterized (subsample B'), 57 of which are in common with MSS11 (subsample C'). A further subdivision for the field sample (subsamples D and E; 162 and 159 stars) based on stars in common with the ELODIE subsample (the reference system in C07) is applied to minimize systematic uncertainties associated with the literature homogenization process in C07.

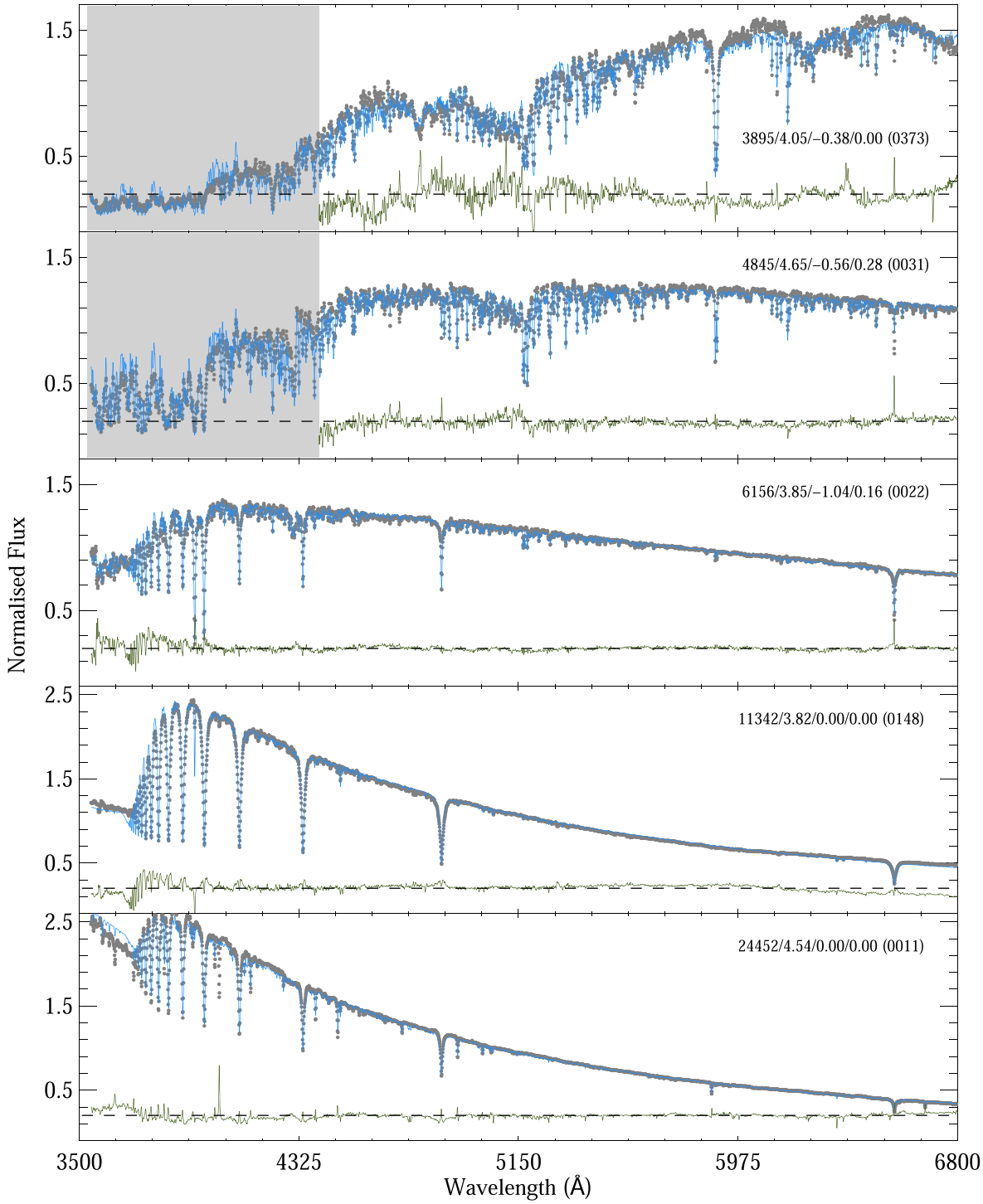


**Figure 5.** Spectra of stars with $\log g > 3.8$, showing observations in grey and their best-fitting model spectra in blue. The stars are presented in order of increasing effective temperature (top to bottom). The residuals ($\frac{\text{Syn}-\text{Obs}}{\text{Obs}}$) scaled by a factor of 1.5 and shifted by 0.2 (for clarity) are presented in green and are accompanied by a dashed line representing zero residuals levels. The stellar parameters are given as $T_{\rm eff}$/log $g$/[Fe/H]/[$\alpha$/Fe] accompanied by the MILES number identification. The shadow in grey shows the spectral region masked out from the analysis. Note that the mask is only applied to the coolest stars (see Section 3.1 for details).

The comparison reveals trends with [Fe/H], as illustrated in Fig. 9. One interesting feature in the metal-rich regime is the tendency for lower metallicities than in the literature, and the existence of an inflection point at [Fe/H] $\sim -1$. At larger metallicities, $\Delta$[Fe/H] and $\Delta$[$\alpha$/Fe] seem to show an inverse correlation. The inflection point coincides with that seen around [Fe/H] $\sim -1$ for the MSS11 pattern. However, unlike in this study, their [Mg/Fe] estimates reach higher values than those obtained at lower metallicities (see their fig 10, with most of these high values coming from their medium-resolution analysis). The strength of the present parameter estimates

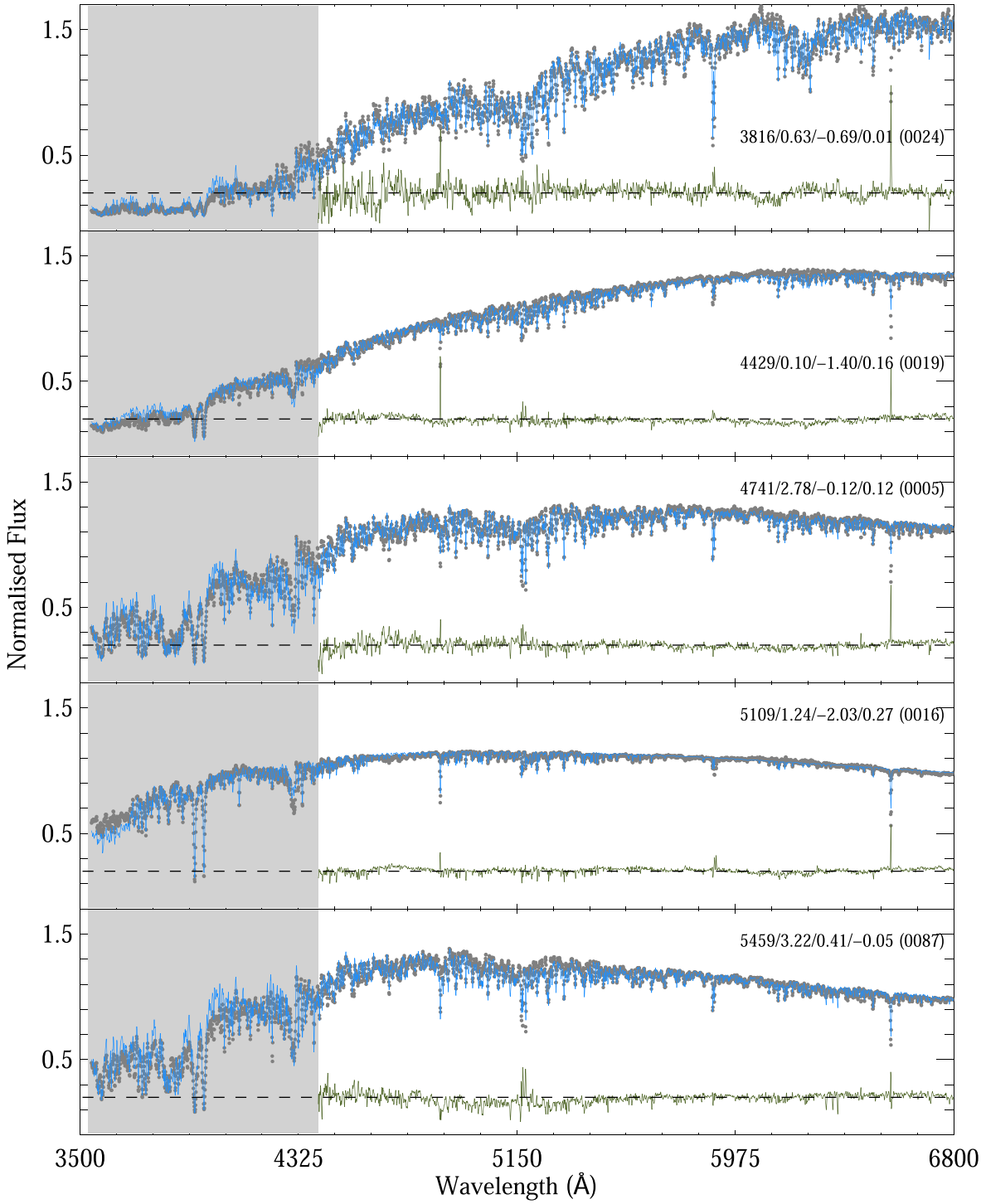


**Figure 6.** Observed and best-fitting spectra as in Fig. 5 but for stars with $\log g < 3.8$.

**Table 5.** Photospheric parameters and abundances of two candidate solar analogues.

| Name | $T_{\rm eff}$ | $\log g$ | [Fe/H] | [$\alpha$/Fe] | $\xi_{\rm t}$ |
|---|---|---|---|---|---|
| HD010307 | 5910 | 4.41 | +0.01 | −0.20 | 1.06 |
| HD095128 | 5819 | 4.22 | −0.02 | −0.19 | 1.00 |

is their homogeneity, with caveats from the use of moderate spectral resolution, while a significant fraction of the estimates provided in C07 compilation come from H–R determinations. Besides, there may be other factors contributing to the differences between these two studies, e.g. the $T_{\rm eff}$ scale, the line list data, the methodologies, etc.

The best agreement between the C07 and the newly derived parameters is found for the cooler stars in the sample (<8000 K), with only small offsets (in the sense of FERRE − C07) of 42 K for

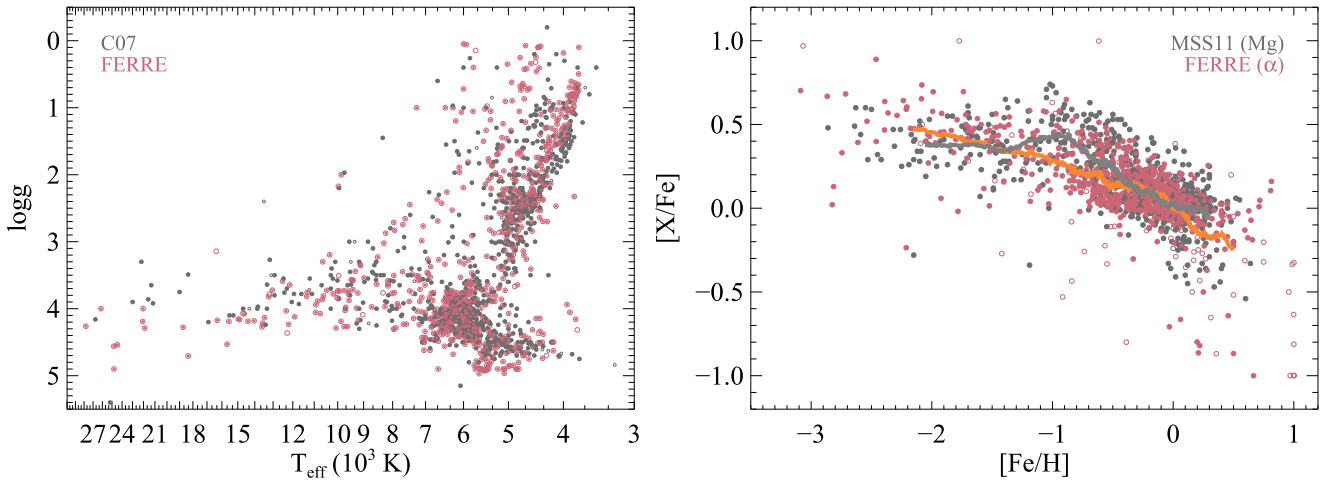


**Figure 7.** Left: H–R diagram of the field sample (sample A). Our work is presented in red, and the literature values of C07 are in grey. The filled symbols denote stars with a complete characterization in C07 ($T_{\rm eff}$, log $g$, and [Fe/H]). Right: Evolution with metallicity of the $\alpha$-element/Fe abundance ratios for sample A. Colours and symbols are as in the left-hand panel, but the full characterization also includes the [Mg/Fe] abundance determinations, which in our case are [$\alpha$/Fe] corrected with the offset derived through the comparison with solar analogues (see Section 4.1 for details). The orange (FERRE) and grey (MSS11) curves shown have been smoothed with a 51-points wide boxcar.

**Table 6.** Photospheric parameters and abundances estimates for field stars in MILES accompanied by their associated FERRE uncertainties, a flag describing the quality of the parameters (see Section 4), and the MILES numeric identification. A full version of this table is available online.

| Name | $T_{\rm eff}$ | log $g$ | [Fe/H] | [$\alpha$/Fe] | log $\xi_{\rm t}$ | $\sigma_{\rm F}T_{\rm eff}$ | $\sigma_{\rm F}$log $g$ | $\sigma_{\rm F}$[Fe/H] | $\sigma_{\rm F}$[$\alpha$/Fe] | $\sigma_{\rm F}$log $\xi_{\rm t}$ | Flag | MILES |
|---|---|---|---|---|---|---|---|---|---|---|---|---|
| BD+002058A | 6145.03 | 4.08 | −1.24 | +0.23 | +0.01 | 2.621 | 0.01 | 0.02 | 0.01 | 0.03 | 1 | 272 |
| BD+012916 | 4385.67 | 0.08 | −1.79 | +0.53 | +0.38 | 6.615 | 0.01 | 0.02 | 0.01 | 0.00 | 1 | 505 |
| BD+044551 | 6047.77 | 3.98 | −1.22 | +0.29 | +0.10 | 2.229 | 0.01 | 0.01 | 0.01 | 0.02 | 1 | 777 |
| BD+053080 | 4844.44 | 4.54 | −0.96 | +0.49 | +0.24 | 1.535 | 0.01 | 0.01 | 0.00 | 0.01 | 1 | 569 |
| BD+060648 | 4428.51 | 0.10 | −2.05 | +0.40 | +0.34 | 0.484 | 0.00 | 0.00 | 0.01 | 0.00 | 11 | 142 |
| BD+062986 | 3909.01 | 4.61 | −1.32 | +0.37 | +0.00 | 0.618 | 0.00 | 0.00 | 0.00 | 0.00 | 0 | 537 |
| BD+090352 | 6276.22 | 4.48 | −1.96 | +0.38 | +0.17 | 3.788 | 0.03 | 0.05 | 0.04 | 0.08 | 1 | 596 |
| BD+092190 | 6455.28 | 4.07 | −3.09 | +0.70 | −0.26 | 5.736 | 0.03 | 0.66 | 0.64 | 0.35 | 1 | 348 |
| BD+093223 | 5424.29 | 2.08 | −2.21 | +0.59 | +0.36 | 1.968 | 0.02 | 0.02 | 0.03 | 0.01 | 1 | 607 |
| BD+112998 | 5365.94 | 2.04 | −1.51 | +0.49 | +0.39 | 2.055 | 0.02 | 0.01 | 0.01 | 0.01 | 1 | 598 |

$\Delta T_{\rm eff}$ and typically below 0.05 for the remaining parameters. For warmer stars, the average difference is larger: +341 K for the $\Delta T_{\rm eff}$ and below 0.14 dex for $\Delta$log $g$; the abundances of hot stars were set to solar. The statistics are reported in Table 7, including the median values, the median absolute deviation, MAD,[6] and a robust measurement of the dispersion based on excluding outliers:

$$\sigma_{\rm r} = \frac{85^{\rm th}\ \text{percentile} - 15^{\rm th}\ \text{percentile}}{2}. \quad (1)$$

The table includes the mean offset ($\mu$) and dispersion ($\sigma_{\rm B}$). These were determined through an MCMC procedure, fitting the data to a t-Student probability distribution that takes into account individual error bars, using the FERRE uncertainties, plus an additional actual dispersion. Not all the cool stars in the sample show deviation from the C07 values of the same sign. The dispersion in the offsets amount to 110 (689) K, and 0.30 (0.36), 0.25, and 0.17 dex for $\Delta T_{\rm eff}$, $\Delta$log $g$, $\Delta$[Fe/H], and $\Delta$[$\alpha$/Fe] (the values for hot stars are given in parenthesis when they differ from those for cooler ones). The dispersion for surface gravity is significant, as illustrated in Fig. 8. There are five stars that lie outside the $y$-axis range of the figures: HD 55693, HD 63302, HD 89822B, HD 187216, and HD 213307. Their offsets have been rescaled to fit in the figure. In our analysis, two of these stars, HD 89822B and HD 213307, appear warmer than in C07. Interestingly, that was also suggested by Prugniel et al. (2011), which further support our new results. Regarding metallicity, HD 187216 is a carbon-rich star (Kipper & Jorgensen 1994), hence our high metallicity estimate is not so surprising because the assumed [C/Fe] = 0. Stars with $T_{\rm eff}$ > 8000 K appear slightly warmer than in C07. They have larger offsets than the cool stars, Fig. 8 shows broader histograms. The Bayesian analysis shows that the two samples have a different behaviour regarding their deviation from C07 parameters, differing on average by −195 K ([−300, −94.6] HDI) and −0.19 dex ([−0.28, −0.10] HDI) in $\Delta T_{\rm eff}$ and $\Delta$log $g$, respectively. Fortunately, the bulk of MILES stars are not in that $T_{\rm eff}$ range. The impact of these hot stars and their uncertainties on stellar population predictions needs to be investigated.

We supplement the distinction between cool and warm stars with a finer $T_{\rm eff}$ division (see Fig. 10). Stars of intermediate $T_{\rm eff}$ (7500–9250 K) stand out because of their larger variations in the discrepancies with the literature metallicity and [$\alpha$/Fe]. Many of them are classified as F, A, B peculiar and Am stars. However, given the small sample included in this bin, the larger spread in the [$\alpha$/Fe] parameter does not imply any significant effect.

[6]Following the usual procedure, to make MAD consistent with the standard deviation of the normal distribution, it has been multiplied by a factor 1.4826.

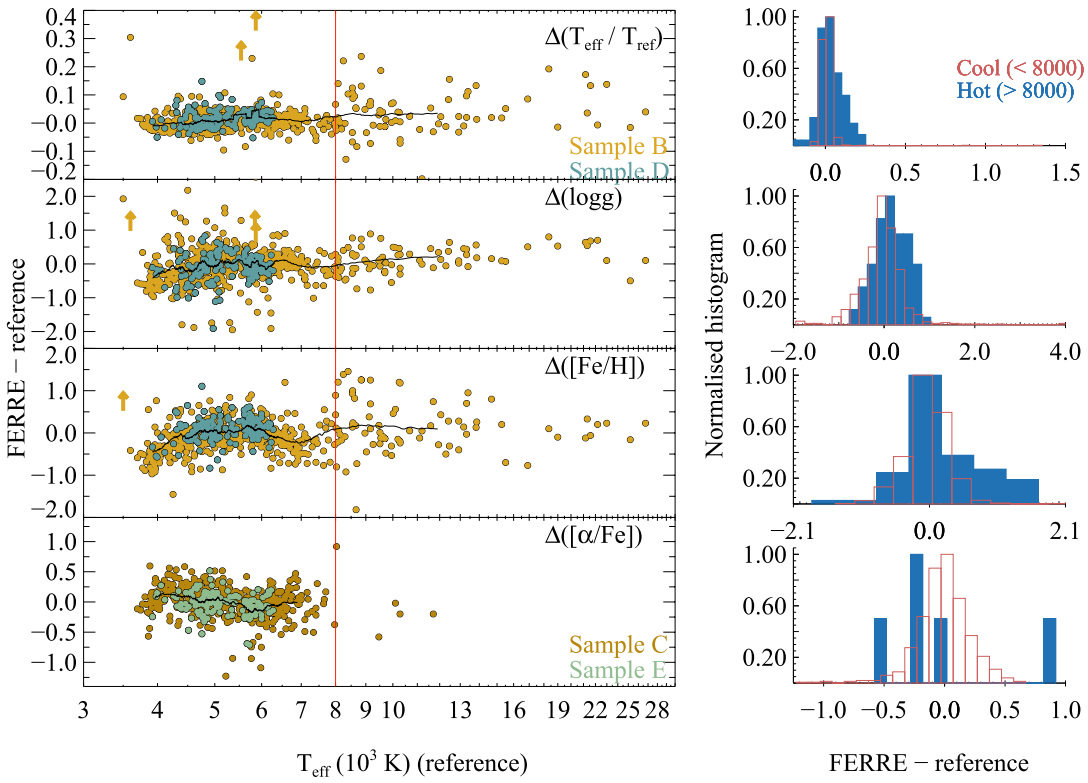


**Figure 8.** Left: Parameter offsets (FERRE − literature) as a function of $T_{\rm eff}$ for the fully characterized samples in C07 (goldenrod) and, for the [$\alpha$/Fe] comparison, in MSS11 (dark goldenrod). For the effective temperature, the offsets are given for $\frac{T_{\rm eff}}{T_{\rm ref}}$ (i.e. $\frac{T_{\rm eff}}{T_{\rm ref}} - 1$). C07 values are presented in the $x$-axis and the stars in common with ELODIE are highlighted in green (lighter in the [$\alpha$/Fe] panel). The data are accompanied by the running mean (51 points size). Arrows refer to data points that have been rescaled in the $y$-axis by a fourth to fit in the figure. Right: Offset histograms for the hot (blue) and cool stars (red). A cool/hot division at 8000 K and a minimum effective temperature of 3750 K are adopted along with bin sizes of 0.05, 0.2, 0.5 (0.3), and 0.1 dex (from the top to the bottom), values for the hot sample are given between parenthesis. Note that our metallicity and abundance values are fixed to zero for the hot stars, which is not necessarily the case for the literature values, thus leading to a difference.

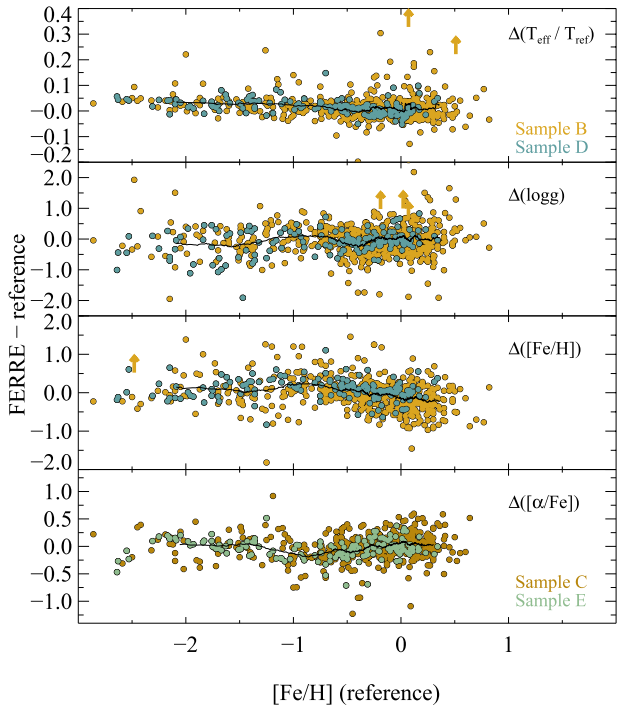


**Figure 9.** Same as in the left-hand panel of Fig. 8 but versus [Fe/H].

### 5.2 Cluster stars

The main motivation for separating discussion of clusters from field stars was their different characteristic chemical compositions and the lower quality (lower S/N) spectra of cluster stars. Moreover in C07, the abundance characterizations were previously averaged for each cluster. The comparison of our results with the C07 + MSS11 characterization for cluster stars is not so different to that for cool field stars. These are presented in Table 8.

Cluster-by-cluster comparison is provided in Table 9 and Fig. 11. The mean offsets in parameters derived for the cluster samples are: $\Delta T_{\rm eff} = -19$ K, $\Delta$[Fe/H] $= -0.04$ dex, $\Delta \log g = -0.21$ dex, and $\Delta$[$\alpha$/Fe] $= -0.06$ dex. The first two of these are not significantly different from 0. However, we detect small, but significant, systematic offsets, in the case of the latter two parameters. These figures do not include the three hottest stars. The conclusions do not change when the analysis is limited to the clusters with more members (M71, NGC 7789, and Hyades).

It is important to note that on average the sample of cluster stars is cooler and has a lower signal-to-noise ratio than our field stars. None the less, comparison of the metallicities as a function of effective temperature and S/N (see Fig. 12) does not reveal any obvious trend with spectral quality. We see similar trends in these clusters as those found for field stars. However, simulations at S/N = 30 suggest that the uncertainties of the photospheric parameters are approximately tripled in comparison to that of S/N = 100.

**Table 7.** Statistics for the comparison to the C07 characterization (FERRE − C07) for cool and hot field stars (division at 8000 K). Median, median absolute deviation, and a robust measurement of the dispersion are given. In addition, the mean value and the dispersion of the $t-$ *student* distribution of the parameter offsets are provided along with the 95 per cent HDI. The sample for the [$\alpha$/Fe] comparison was reduced to 642 and 5 stars for the cool and hot subsamples, respectively.

| | $\Delta T_{\rm eff}$ | | $\Delta \log g$ | | $\Delta$[Fe/H] | | $\Delta$[$\alpha$/Fe] | | $N$ | |
|---|---|---|---|---|---|---|---|---|---|---|
| | Cool | Hot | Cool | Hot | Cool | Hot | Cool | Hot | Cool | Hot |
| Median | +44.2 | +278.2 | −0.04 | +0.11 | −0.03 | 0.10 | −0.00 | −0.20 | 693 (642) | 79 (5) |
| MAD | 132.3 | 652.7 | 0.33 | 0.36 | 0.25 | 0.44 | 0.17 | 0.27 | 693 (642) | 79 (5) |
| $\sigma_{\rm r}$ | 137.4 | 786.7 | 0.39 | 0.39 | 0.29 | 0.60 | 0.19 | 0.75 | 693 (642) | 79 (5) |
| $\mu$ | +42.2 | +341 | −0.05 | +0.14 | −0.04 | ... | −0.01 | ... | 693 (642) | 79 (5) |
| $\sigma_{\rm B}$ | 110.0 | 689.0 | 0.30 | 0.36 | 0.25 | ... | 0.16 | ... | 693 (642) | 79 (5) |
| HDI ($\mu$) | (+33.0, +52.9) | (+155, +550) | (−0.07, +0.02) | (+0.06, +0.22) | (−0.06, −0.02) | ... | (−0.02, +0.01) | ... | 693 (642) | 79 (5) |
| HDI ($\sigma_{\rm B}$) | (101,119) | (479,936) | (0.27,0.33) | (0.30,0.42) | (0.22,0.27) | ... | (0.15,0.18) | ... | 693 (642) | 79 (5) |

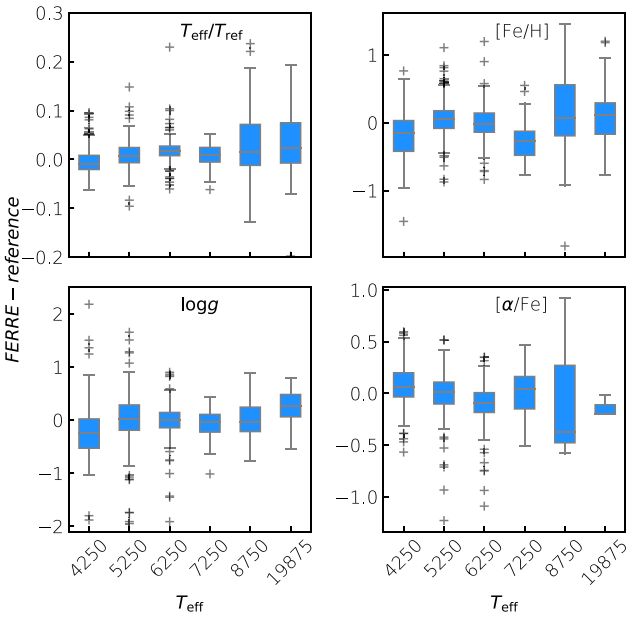


**Figure 10.** Box plots showing departures from the C07 characterization at different $T_{\rm eff}$ bins for the parameters and abundances of the field stars. The box corresponds to the first and third quartiles, the caps show the extension to the 1.5× interquartile range, and the horizontal bar indicates the median value. Outliers are shown with plus symbols, some of them lie outside the axis ranges.

The Hyades members include warm $T_{\rm eff}$s and high S/N stars, and there is good agreement with the C07 + MSS11 results for this cluster. NGC 7789 (e.g. Jacobson, Pilachowski & Friel 2011; Donor et al. 2018) shares $T_{\rm eff}$ range with M71 (e.g. Ramírez, Cohen, Buss & Briley 2001; Mészáros et al. 2015), but despite higher spectral quality data, we find no obvious indication of a better agreement in the former cluster, perhaps due to its higher metallicity. Another interesting example is NGC 6791 (e.g. Cunha et al. 2015), for which a combination of very low $T_{\rm eff}$ and *S/N* values in the metal-rich regime could be responsible for the discrepancies we find. In fact only two stars (out of four) that did not hit the low-temperature cut-off of the model grid were used for this comparison, leading to the largest departure from C07 parameters among all the clusters. That combination of low temperatures and high noise also seems to impact results at low metallicity. For example, a large $\Delta \log g$ of −0.71 dex (median value) is measured for M92, our most metal-poor globular cluster. Based on the goodness-of-fit, we have no strong reason to discard our cluster results. A comparison of models and data for the Hyades ([Fe/H] ∼ +0.13) is presented in Fig. 13.

### 5.3 Parameter uncertainties

Clusters are ideal labs for validating abundance determinations. However, given the lower S/N of the cluster star spectra, the spread in metallicity can be taken as a conservative error estimate. Such uncertainties could be adopted for the entire MILES sample, although it is known that there are multiple populations in globular clusters, and that both globular clusters and old open clusters are affected by diffusion (e.g. Korn et al. 2007; Souto et al. 2018). The typical metallicity dispersion for the cluster sample exceeds the FERRE uncertainties quoted for field stars, <0.05 dex. Our best statistically sampled clusters are M71, NGC 7789, and Hyades, with at least 14, 10, and 12 stars each (see Table 7). They cover S/N in the range of 10–100 (M71; 10–50), and mostly, temperatures of 3900–6000 K (Hyades; 5530–9688 K). The typical [$\alpha$/Fe] dispersion of ∼0.1–0.2 dex measured in these clusters is larger than the typical FERRE uncertainties of < 0.02, but the former can include real variations of the $\alpha$-content within the cluster. However, these quoted cluster values are not so different to the averaged values listed for the C07 comparison of the cool field sample and we use the latter to constrain our uncertainties. Assuming our results are at least as good as those in C07, we can obtain a conservative estimate of our uncertainties using the $\sigma_{\rm B}$ values given in Table 7. These values are associated with the MCMC analysis, explained in Section 5.1, of the 693 field stars and were divided by $\sqrt{2}$ to account for a two studies comparison. Final error bars of $\sigma_{\rm t}(T_{\rm eff}) = 78$ K, $\sigma_{\rm t}$ (log $g$) = 0.21 dex, $\sigma_{\rm t}$([Fe/H]) = 0.18 dex, and $\sigma_{\rm t}$([$\alpha$/Fe]) = 0.11 dex are estimated. Hot stars are expected to have larger $T_{\rm eff}$ error bars.

## 6 OVERLAPS WITH OTHER SURVEYS

MILES has a significant number of stars in common with APOGEE (93 in the field and 20 in clusters). Only those stars with good (calibrated) estimates in the SDSS 14th Data Release (DR14th; Abolfathi et al. 2018) are selected for comparison: a total of 45 field stars (sample I) in a $T_{\rm eff}$ range of 3990–5445 K. Furthermore, the APOGEE survey is based on a different spectral range (the *H* band), and their estimates have been calibrated to a fundamental scale, e.g. based on asteroseismic values for log $g$ and thus good agreement with this survey would add value to this study.

Indeed, the agreement between the two studies is good in terms of average offsets, as illustrated in Fig. 14. The typical differences seem to be negligible in terms of what is typically found for similar

**Table 8.** Photospheric parameters and abundance estimates of cluster stars accompanied by their associated FERRE uncertainties, a flag describing the quality of the estimates (see Section 4), and the MILES numeric identification. A full version of the table is available online.

| Cluster | Name | $T_{\rm eff}$ | log $g$ | [Fe/H] | [$\alpha$/Fe] | log $\xi_{\rm t}$ | $\sigma_{\rm F}T_{\rm eff}$ | $\sigma_{\rm F}$log $g$ | $\sigma_{\rm F}$[Fe/H] | $\sigma_{\rm F}$[$\alpha$/Fe] | $\sigma_{\rm F}$log $\xi_{\rm t}$ | Flag | MILES |
|---|---|---|---|---|---|---|---|---|---|---|---|---|---|
| AlphaPer | HD020902 | 6313.26 | 2.00 | −0.79 | +0.37 | +0.69 | 4.115 | 0.03 | 0.01 | 0.01 | 0.00 | 0 | 898 |
| ComaBer | HD107276 | 8090.10 | 3.94 | −0.29 | +0.20 | +0.40 | 2.351 | 0.00 | 0.01 | 0.01 | 0.01 | 1 | 920 |
| ComaBer | HD107513 | 7455.42 | 4.09 | −0.47 | +0.21 | +0.60 | 3.362 | 0.01 | 0.01 | 0.01 | 0.01 | 1 | 921 |
| ComaBer | HD109307 | 8399.79 | 3.67 | −0.11 | −0.17 | +0.54 | 7.018 | 0.01 | 0.02 | 0.03 | 0.01 | 1 | 922 |
| NGC 2420 | NGC 2420-140 | 4315.10 | 1.51 | −0.37 | +0.17 | +0.16 | 1.804 | 0.01 | 0.01 | 0.01 | 0.00 | 1 | 918 |
| NGC 288 | NGC 288-77 | 4381.08 | 0.10 | −0.78 | +0.16 | +0.14 | 4.056 | 0.00 | 0.01 | 0.02 | 0.01 | 11 | 897 |
| NGC 6791 | NGC 6791-R4 | 3668.61 | 1.81 | +0.66 | +0.17 | +0.00 | 1.605 | 0.02 | 0.01 | 0.00 | 0.00 | 00 | 940 |
| NGC 6791 | NGC 6791-R5 | 3500.00 | 4.91 | +0.50 | +0.68 | +0.33 | 0.000 | 0.02 | 0.11 | 0.04 | 0.02 | 4 | 941 |
| NGC 6791 | NGC 6791-R16 | 3804.43 | 1.11 | −0.53 | +0.05 | +0.20 | 1.723 | 0.01 | 0.01 | 0.00 | 0.01 | 1 | 942 |
| NGC 6791 | NGC 6791-R19 | 3765.01 | 1.18 | −0.62 | +0.01 | +0.21 | 1.871 | 0.01 | 0.01 | 0.00 | 0.01 | 1 | 943 |

**Table 9.** Statistics for the comparison with the C07 characterization in clusters, median values are accompanied by the standard deviation, the MAD, and the number of data points used. The sample size for the $\alpha$ comparison, if different to that of the rest of the comparison, is given between parenthesis.

| Cluster | [Fe/H] | $\Delta T_{\rm eff}$ | | | $\Delta$log $g$ | | | $\Delta$[Fe/H] | | | $\Delta$[$\alpha$/Fe] | | | N (for [$\alpha$/Fe]) |
|---|---|---|---|---|---|---|---|---|---|---|---|---|---|---|
| | C07 | Median | $\sigma$ | MAD | Median | $\sigma$ | MAD | Median | $\sigma$ | MAD | Median | $\sigma$ | MAD | |
| M92 | − 2.16 | +177.5 | 14.6 | 30.5 | − 0.71 | 0.11 | 0.22 | − 0.07 | 0.17 | 0.35 | − 0.05 | 0.03 | 0.05 | 2 (2) |
| M13 | − 1.39 | − 75.7 | 391.4 | 820.5 | − 0.29 | 0.48 | 1.01 | +0.32 | 0.50 | 1.06 | +0.02 | ... | ... | 2 (1) |
| M79 | − 1.37 | +192.6 | 28.6 | 19.5 | − 0.54 | 0.10 | 0.13 | +0.06 | 0.11 | 0.06 | − 0.30 | 0.06 | 0.13 | 3 (2) |
| M3 | − 1.34 | +147.3 | 40.6 | 30.4 | − 0.67 | 0.07 | 0.11 | − 0.17 | 0.10 | 0.03 | +0.24 | 0.11 | 0.16 | 3 (3) |
| M5 | − 1.11 | +59.5 | 106.5 | 14.3 | − 0.20 | 0.95 | 0.51 | +0.15 | 0.14 | 0.10 | − 0.13 | ... | ... | 3 (1) |
| M71 | − 0.84 | − 62.9 | 275.2 | 132.2 | − 0.12 | 0.55 | 0.49 | +0.17 | 0.31 | 0.31 | − 0.33 | 0.16 | 0.19 | 23 (15) |
| NGC 7789 | − 0.13 | − 234.3 | 66.7 | 46.3 | − 0.11 | 0.60 | 0.34 | − 0.33 | 0.24 | 0.26 | − 0.03 | 0.15 | 0.21 | 12 (11) |
| ComaBer | − 0.05 | +46.4 | 95.6 | 106.3 | − 0.27 | 0.17 | 0.16 | − 0.24 | 0.18 | 0.26 | − 0.10 | 0.02 | 0.04 | 3 (2) |
| Pleiades | − 0.03 | +28.1 | 108.8 | 228.0 | − 0.11 | 0.15 | 0.32 | − 0.29 | 0.22 | 0.46 | +0.39 | 0.05 | 0.10 | 2 (2) |
| Hyades | +0.13 | +48.0 | 231.9 | 103.8 | − 0.02 | 0.27 | 0.27 | − 0.08 | 0.27 | 0.24 | − 0.04 | 0.18 | 0.08 | 14 (13) |
| NGC 6791 | +0.40 | − 279.8 | 58.3 | 122.2 | − 0.58 | 0.15 | 0.31 | − 0.97 | 0.07 | 0.14 | +0.42 | ... | ... | 2 (1) |

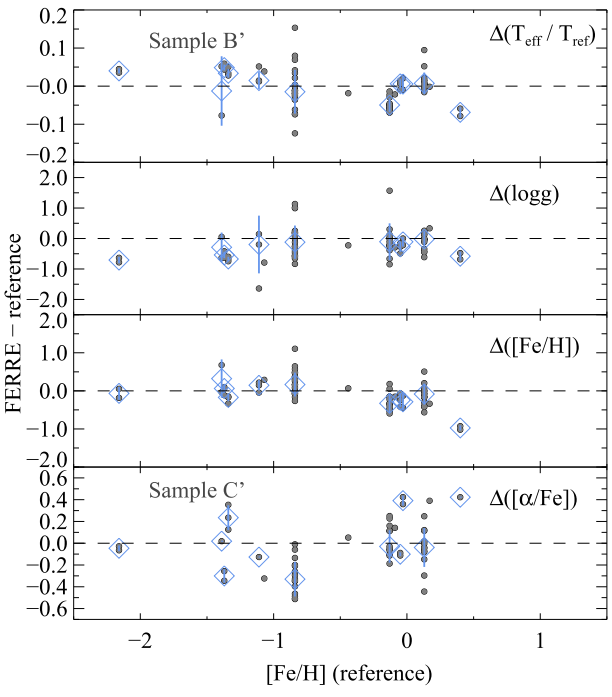


**Figure 11.** A comparison of the current metallicity determinations to the values in C07 for MILES clusters. Points represent differences (FERRE − reference) for the individual stars. Diamonds and bars indicate the respective median values of all the stars in the individual clusters and the dispersion (standard deviation), respectively. Samples in common with C07 and with MSS11 are presented.

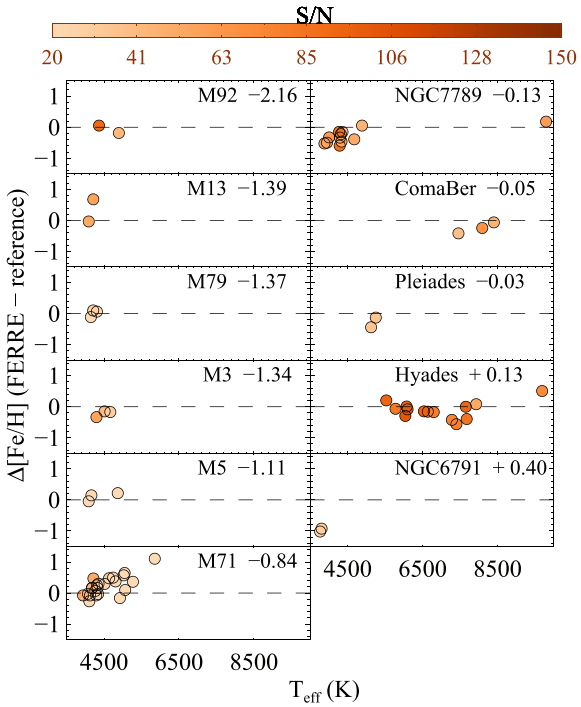


**Figure 12.** Metallicity differences between this study and C07 as a function of effective temperature and S/N (colour coded). Individual stars in clusters of different metallicities are presented. The dashed line indicates a null offset, and the values in the legend correspond to the CO7 metallicity estimates.

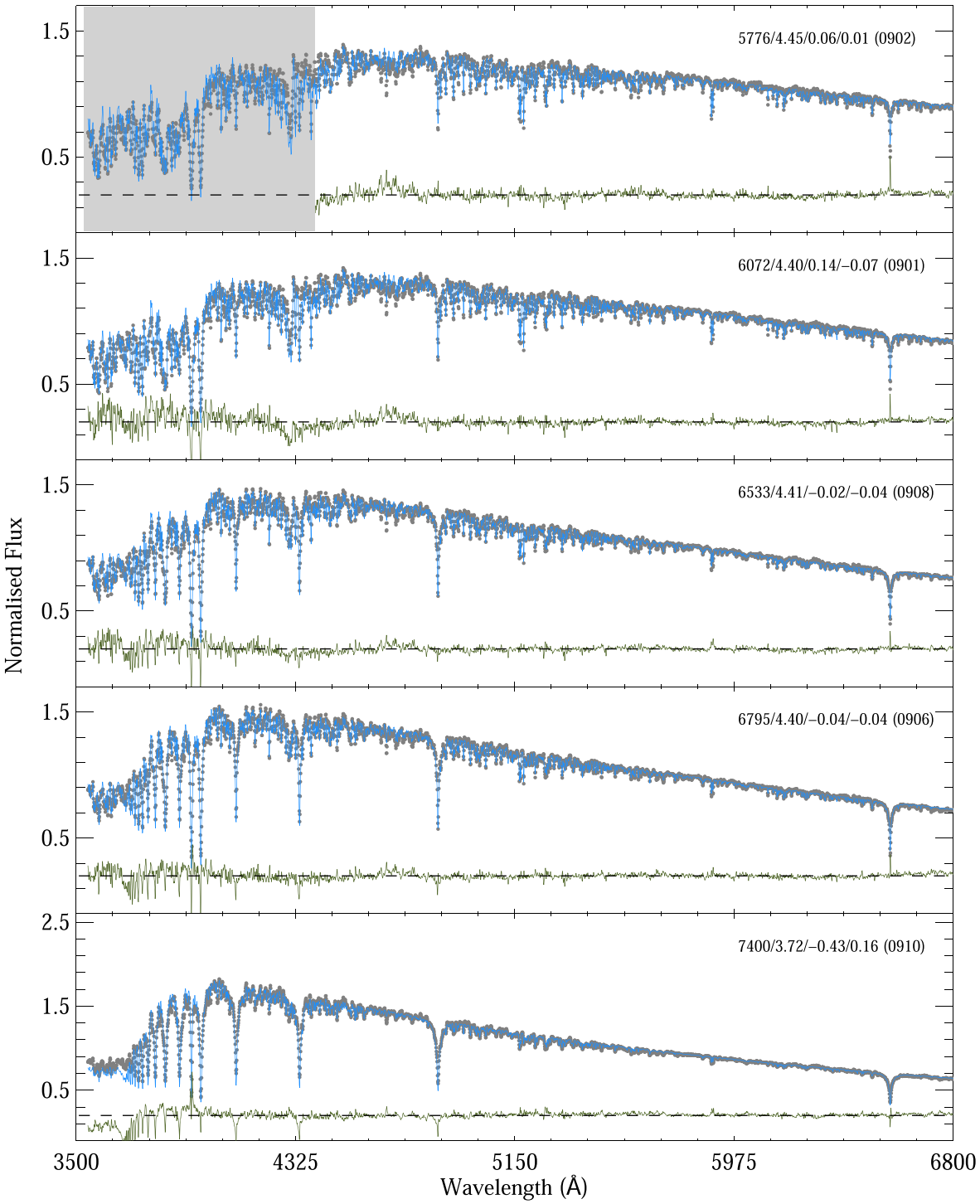


**Figure 13.** Observed (grey) and best-fitting (blue) spectra of five stars of the open cluster Hyades ([Fe/H] $\sim +0.13$).

type of comparisons in the literature. In particular, we have derived two estimates of the offsets between both sources: (i) simple median offsets, and (ii) estimates of the mean offsets and their uncertainties using a Bayesian approach with MCMC, as in Sections 2.2 and 5.1 (these are the values quoted within Fig. 14). The corresponding offsets are respectively: $\Delta T_{\rm eff} = (-47, -71.2)$ K, $\Delta \log g = (-0.09, -0.12)$ dex, $\Delta$[Fe/H] $= (-0.11, -0.09)$ dex, and $\Delta[\alpha/{\rm Fe}] = (+0.12, +0.11)$ dex. On the other hand, the dispersion ($1\sigma_{\rm r}$) around these differences derived by the second approach is significant: 144 K, 0.37 dex, 0.31 dex, and 0.13 dex, respectively for the four parameters. The Bayesian analysis indicates that the [$\alpha$/Fe] offset is significantly different from zero, with a 95 per cent HDI of $(+0.08, +0.15)$. For the other parameters, the zero offset is within the 95 per cent HDI: $(-105.0, +33.1)$, $(-0.25, +0.00)$, and $(-0.18, -0.01)$ for $\Delta T_{\rm eff}$, $\Delta \log g$, and $\Delta$[Fe/H], respectively. In addition, all the four parameters do require an extra source of uncertainty of 100 K ($\sigma_{T_{\rm eff}}$), 0.36 ($\sigma_{\log g}$), 0.27 ($\sigma_{\rm [Fe/H]}$, and 0.09 dex ($\sigma_{[\alpha/{\rm Fe}]}$ to account for the observed dispersion.

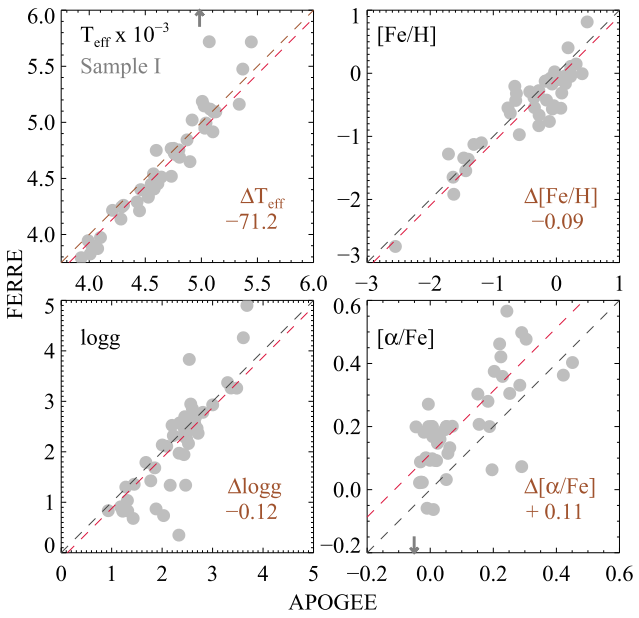


**Figure 14.** A comparison of MILES parameters versus the APOGEE results (DR14 values) for a common sample of 45 field stars (sample I; circles). Grey and red lines indicate the 1:1 relation and the mean departure from it (based on the Bayesian analysis; see the values given in the legend). The arrows mark the *x* positions of two outliers that do not fit in the adopted *y* scale.

APOGEE is a high spectral resolution survey in the IR, while MILES observes in the optical and at a middle spectral resolution. Furthermore, our analysis does not consider carbon and nitrogen abundances individually, in contrast with APOGEE, hence our metallicity estimates may be accounting for these abundances. The analyses can be affected by these sources of discrepancy, e.g. zero-points offsets, delivering results on a different scale. Our new estimates may not be as accurate as APOGEE but they have an advantage over the C07 because they are consistently determined from the MILES observations. The C07 parameters seem to agree slightly better with APOGEE than ours, however, the difference is not statistically significant.

The literature has other studies in common with MILES stars, e.g. the high spectral resolution analysis of the *Gaia* FGK Benchmark Stars (GBS) by Jofré et al. (2018), or that of the Milky Way disc by Bensby, Feltzing & Oey (2014). The agreement with them is similar to that with C07. The parameters determined here show slightly larger $\log g$ and [Fe/H] offsets, but with lower dispersion; $\Delta \log g \sim -0.05$ and $\Delta$[Fe/H] $-$ 0.10 (for GBS) with a dispersion of ∼0.22 and ∼0.15 (MAD), respectively. Note that smaller MILES subsamples are being compared in contrast to the C07 comparison. Interestingly, our agreement with the studies of Sharma et al. (2016) and Prugniel et al. (2011) is not much better, despite the fact that these studies also use the MILES stars themselves, as performed here. Note, however, their analyses are based on empirical models rather than on theoretical models. A slightly worse agreement was particularly found for $\log g$ (for Sharma et al. 2016) and metallicity within 0.25–0.35 dex. It is worth mentioning that Sharma et al. (2016) focus on the cool MILES spectra.

## 7 EXTENDED MILES LIBRARY

The effort to extend the MILES library resulted in an additional 205 spectra, 193 of which (sample J) are incorporated into the current characterization. The remaining stars were excluded due to poor fits (11 stars) and/or too cool temperatures (1 star). Fig. 15 compares models and data for a few example stars. The new parameters along with their FERRE-based uncertainties are given in Table 10, while the final characterization of the entire MILES sample (1070 stars) is presented in Figs 16 and 17. Note that the [$\alpha$/Fe] abundance ratios at $T_{\rm eff} < 5800$ K in the extension, as was the case for the original sample (see Section 4), needs the +0.2 dex correction based on the solar analogues.

The newly added 193 stars are mainly in the range $4000 \lesssim T_{\rm eff}$(K) $\lesssim 6700$ and $-1.2 \lesssim$ [Fe/H] $\lesssim +0.8$. They occupy regions of the H–R diagram already populated by the original MILES library, but enhancing the density on the main sequence (128 stars; $\log g \sim 3.5$–4.9) and the red giant branch (65 stars; $\log g \sim 1.0$–3.5), where it is most profitable for population synthesis studies. The final main sequence ($\log g > 3.5$) is statistically better represented than the red giant branch.

The [$\alpha$/Fe] content shows similar patterns in the three samples (field, clusters, and extension). The [$\alpha$/Fe] ratio increases linearly with decreasing metallicity, in agreement with expectations for stars in the local solar neighbourhood. Contrary to MSS11, we do not find the peak that is seen in the [$\alpha$/Fe] distribution of the original MILES sample at [Fe/H] $\sim -1.0$. However, like in MSS11, we observe a flattening in the abundance distribution at lower metallicities. This flattening is not only supported by the running mean curve shown in Fig. 7 but also by a non-linear regression based on a cubic splines fitting.

The extended sample has enhanced, although modestly, the range in [$\alpha$/Fe] (see Fig. 17). More importantly, the coverage has improved thanks to a more dense observational data set of chemical compositions. In the range $-1.0 \lesssim$ [Fe/H] $\lesssim +0.6$, [$\alpha$/Fe] is slightly lower, the middle boxes in Fig. 18 extend down by typically <0.1 dex with respect to the original coverage. This was, based on the target selection, expected for the low metallicities. This reflects the importance of a homogeneous determination of the stellar parameters and abundances. Concluding, the additional spectra improve the sample statistics in terms of size and coverage and provides increased [$\alpha$/Fe] and metallicity coverage, particularly in the range above one-tenth of solar metallicity (see Fig. 18). This clearly represents a step forward for modelling stellar populations.

## 8 SUMMARY

Galaxies come in different flavours, e.g. different morphologies, kinematics, and stellar populations. Libraries of stellar spectra are one of the key parameters for delving into knowledge of these populations, e.g. using models of population synthesis to derive some of the main galactic properties. MILES is one of the highest-quality widely used libraries ($R \sim 2000$; S/N > 100). However, the atmospheric parameter characterization relied on a compilation from the literature. The current analysis provides a uniform analysis based on theoretical star spectra, the standard approach in stellar spectroscopy.

This homogeneous and new characterization is based on an automated analysis using synthetic spectra to match observations. The study faces difficulties associated with the wide coverage in spectral types (M to OB type), e.g. different methodologies were adopted depending on these characteristics (wavelength masking and reducing the number of fitted parameters at high $T_{\rm eff}$). The final catalogue includes 1070 stars for which all the main four photospheric parameters ($T_{\rm eff}$, $\log g$, [Fe/H], and $\xi_{\rm t}$) plus the $\alpha$/Fe abundance ratio are provided. Importantly, many stars from the

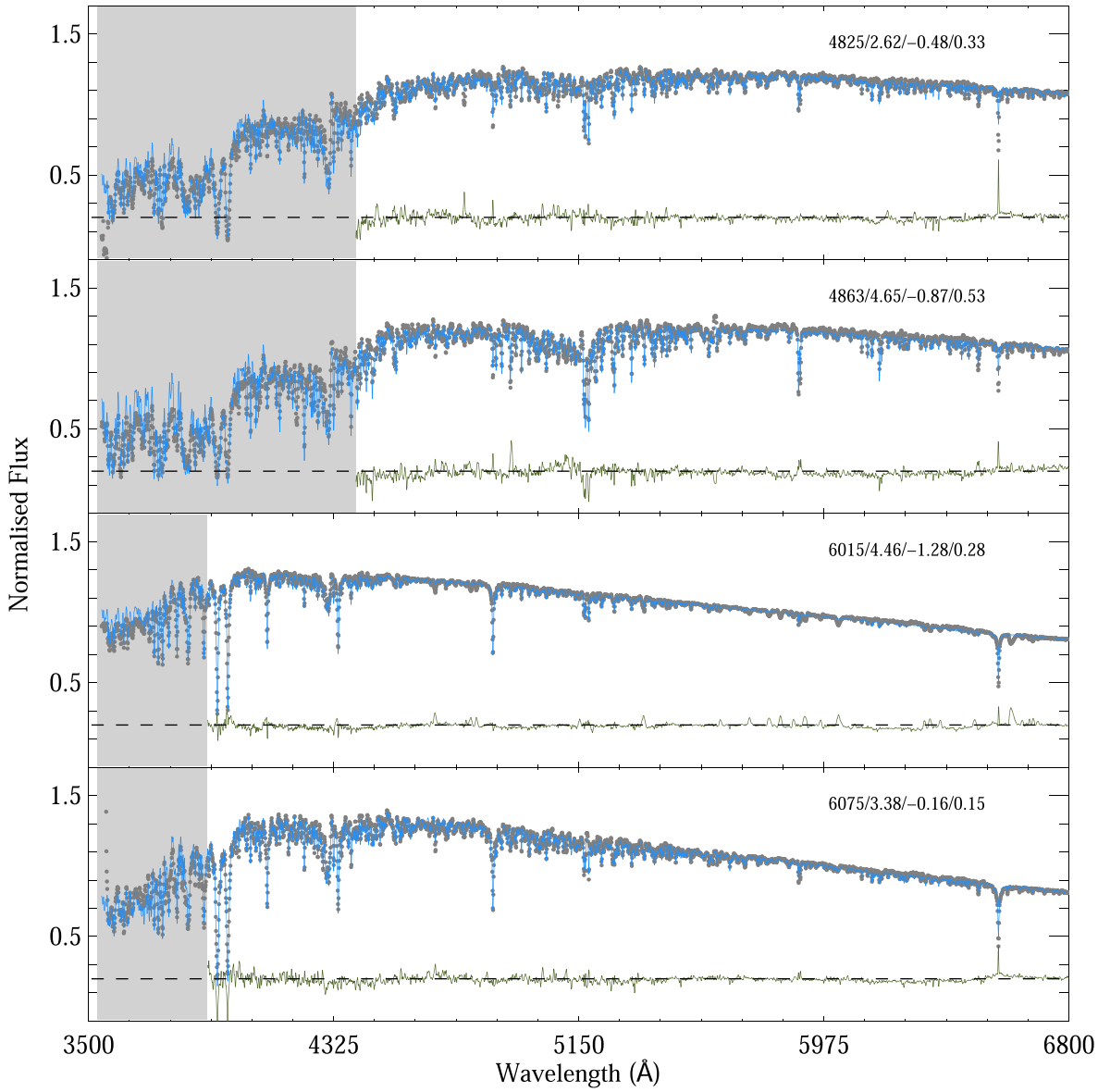


**Figure 15.** Observed and best-fitting spectra as in Fig. 5 but for both giant and dwarf stars of the extra MILES sample.

**Table 10.** Photospheric parameters and abundance estimates of the extra sample accompanied by their associated FERRE uncertainties and a flag describing the quality of the estimates (see Section 4). A full version of the table is available online.

| Name | $T_{\rm eff}$ | log $g$ | [Fe/H] | [$\alpha$/Fe] | log $\xi_{\rm t}$ | $\sigma_{\rm F}T_{\rm eff}$ | $\sigma_{\rm F}$log $g$ | $\sigma_{\rm F}$[Fe/H] | $\sigma_{\rm F}$[$\alpha$/Fe] | $\sigma_{\rm F}$log $\xi_{\rm t}$ | Flag |
|---|---|---|---|---|---|---|---|---|---|---|---|
| BD+194601 | 5594.93 | 4.59 | −0.53 | +0.22 | +0.11 | 10.302 | 0.02 | 0.03 | 0.02 | 0.03 | 1 |
| BD+224454 | 5270.15 | 4.37 | −0.40 | +0.32 | −0.28 | 3.000 | 0.02 | 0.05 | 0.01 | 0.00 | 1 |
| BD+252555 | 5000.11 | 1.73 | −0.40 | −0.06 | +0.11 | 6.729 | 0.04 | 0.02 | 0.03 | 0.02 | 1 |
| BD+334707 | 4867.84 | 4.69 | −0.87 | +0.51 | +0.20 | 1.755 | 0.01 | 0.01 | 0.00 | 0.01 | 1 |
| G056-036 | 6548.94 | 4.90 | −0.38 | −0.31 | −0.29 | 1.702 | 0.00 | 0.04 | 0.02 | 0.00 | 44 |
| G119-064 | 6750.33 | 4.97 | −1.34 | −0.00 | −0.06 | 2.055 | 0.01 | 0.03 | 0.01 | 0.04 | 0 |
| G121-012 | 6379.16 | 4.75 | −0.86 | −0.09 | −0.12 | 2.344 | 0.02 | 0.04 | 0.02 | 0.04 | 1 |
| G159-050 | 5943.07 | 3.66 | −0.62 | +0.32 | +0.00 | 1.378 | 0.01 | 0.00 | 0.01 | 0.00 | 11 |
| G176-053 | 6019.91 | 4.46 | −1.28 | +0.09 | +0.11 | 2.406 | 0.02 | 0.02 | 0.01 | 0.03 | 0 |
| G180-024 | 6673.69 | 4.90 | −0.44 | −0.45 | −0.30 | 1.784 | 0.00 | 0.04 | 0.02 | 0.00 | 22 |

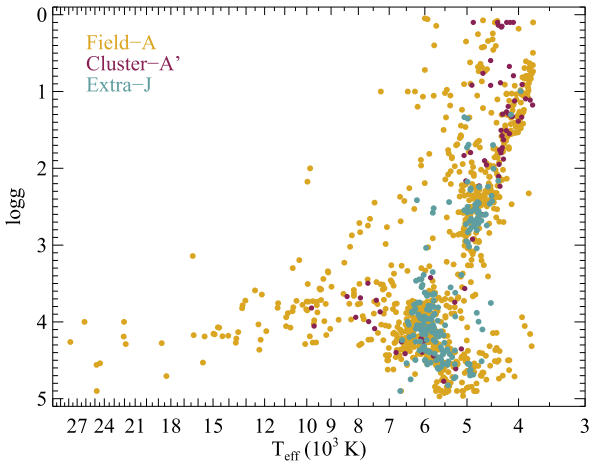


**Figure 16.** Final MILES stellar characterization. H–R diagram for field stars (goldenrod; sample A) along with the new additions (cadet blue; sample J), and cluster stars (maroon; sample A').

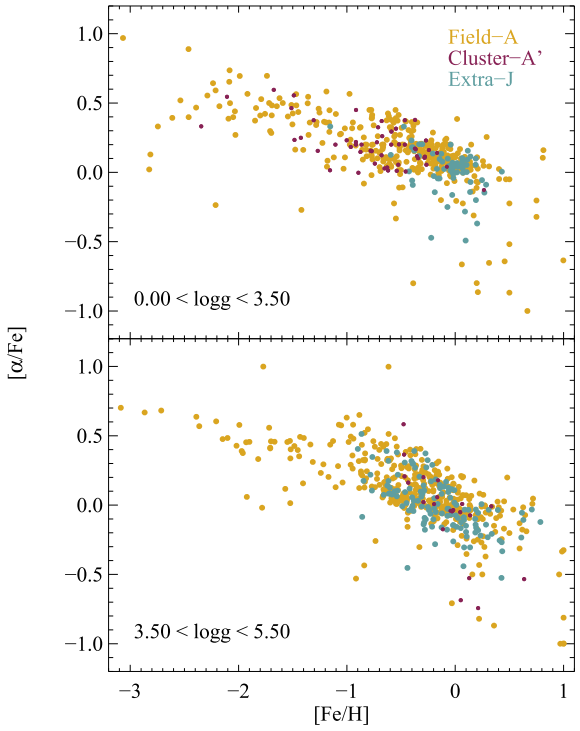


**Figure 17.** Final MILES stellar characterization. The evolution of [$\alpha$/Fe] with metallicity for different samples: giants (top) and main sequence (bottom). Field stars are shown in goldenrod (sample A) and cluster stars in maroon (sample A'), while cadet blue (sample J) denotes the new field stars.

original MILES with incomplete stellar parameter determinations are now fully characterized (119 for $T_{\rm eff}$ < 10 000 K), as a result of the combined analysis of the parameters and abundances. On the other hand, a small sample of the original library is missing complete parameters because of the lower quality of their spectral fits and/or too-low $T_{\rm eff}$ (<3750 K).

The stars analysed typically follow the expected H–R diagram (mainly dwarfs and giants), as well as the typical $\alpha$-content pattern observed for the Local Solar Neighbourhood in the Milky Way galaxy. The new stellar parameters are approximately consistent

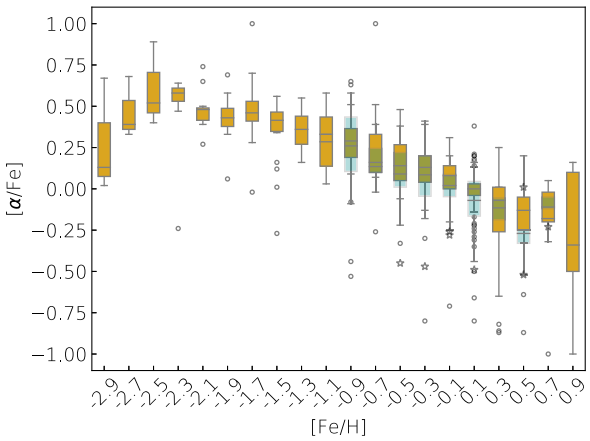


**Figure 18.** Variations of [$\alpha$/Fe] with [Fe/H] for the field stars of the original library (goldenrod) and its extension (cadet blue) in binning of 0.2 in [Fe/H]. Median values, the 25th and 75th percentiles, and the extension to the 1.5× interquartile range are shown by the boxplots. Circles (original) and stars (extension) represent outliers.

with those of C07 and MSS11, and even with IR-based estimates (SDSS/APOGEE). The differences with those catalogues for stars with $T_{\rm eff}$ < 8000 K show a dispersion of 110 K in $T_{\rm eff}$ and 0.2–0.3 dex for the abundances. The largest discrepancies are found for the surface gravities ($\sigma_{\rm r} \sim$ 0.3–0.4 dex).

With the intention to improve the modelling of other galaxies, an additional set of 205 stars have been added to enhance the [Mg/Fe] coverage of the library. These stars were selected based on their literature abundances of Mg. The new 193 stars with a full characterization (the rest did not have good fits) are shown in Figs 16, 17, and 18. The sample increase is particularly important for dwarf stars and resulted in a better coverage of the [$\alpha$/Fe] content, although, limited to the Milky Way abundance pattern. Particularly relevant is the increase in density of stars with varying [$\alpha$/Fe] values at fixed [Fe/H] (see Fig. 18). This allows the construction of models with varying abundance ratios based on the extended MILES stars. Although these predictions can only be made for a limited range of [$\alpha$/Fe], such models will be very useful to test models based on full, or partially, theoretical star spectra. This work is the first component of a large-scale effort to improve stellar population models applicable to a wide range of observations and galaxy types. Both versions of the library (with and without interpolation) along with the uncertainties spectra will be available on http://miles.iac.es/.

## ACKNOWLEDGEMENTS

We thank the referee for a thorough revision that helped us to improve the original draft and the presentation of this work. We are also grateful to E. Mármol-Queraltó for helping us during the observations and to R. Peletier for useful discussions. AEGP, AV, PSB, and JG acknowledge financial support from the coordinated grants AYA2016-77237-C3-1-P, AYA2016-77237-C3-2-P, PID2019-107427GB-C32 and PID2019-107427GB-C31 from the Spanish Ministry of Science, Innovation and Universities (MCIU), while CAP does from AYA2017-86389 (also from the MCIU). ACM was supported by the research grant (309562/2015-5) from the Brazilian National Council for Scientific and Technological Development (CNPq) foundation. He also thanks the Institutional Training Program (PCI) of the Brazilian Ministry of Science, Technology and Innovations (MCTI) at Instituto Nacional de Pesquisas Espaciais

(INPE) (individual process 17.0018/2010-5 under the institutional process 680.006/2009-5) for financial support for the 2011 (run A) observational campaign.

## DATA AVAILABILITY

The data underlying this article will be available on http://miles.iac.es/.

## REFERENCES


Abolfathi B. et al., 2018, ApJS, 235, 42
Allard N. F., Kielkopf J. F., Cayrel R., van't Veer-Menneret C., 2008, A&A, 480, 581
Allende Prieto C., 2011, MNRAS, 411, 807
Allende Prieto C., Beers T. C., Wilhelm R., Newberg H. J., Rockosi C. M., Yanny B., Lee Y. S., 2006, ApJ, 636, 804
Allende Prieto C., Koesterke L., Hubeny I., Bautista M. A., Barklem P. S., Nahar S. N., 2018, A&A, 618, 25
Alonso A., Arribas S., Martínez-Roger C., 1996, A&A, 313, 873
Alves-Brito A., Melendez J., Asplund M., Ramirez I., Yong D., 2010, A&A, 513, 35
Amarsi A. M., Nordlander T., Barklem P. S., Asplund M., Collet R., Lind K., 2018, A&A, 615, A139
Asplund M., Grevesse N., Sauval A. J., 2005, in Barnes III T. G., Bash F. N., eds, ASP Conf. Ser. Vol. 336, Cosmic Abundances as Records of Stellar Evolution and Nucleosynthesis in honor of David L. Lambert. Astron. Soc. Pac., San Francisco, p. 25
Barklem P. S., 2016, A&AR, 24, 9
Beers T. C., Rossi S., Norris J. E., Ryan S. G., Shefler T., 1999, AJ, 117, 981
Bensby T., Feltzing S., Lundström I., Ilyin I., 2005, A&A, 433, 185
Bensby T., Feltzing S., Oey M. S., 2014, A&A, 562, A71
Bertone E., Buzzoni A., Rodríguez-Merino L. H., Chávez M., 2004, Mem. Soc. Astron. Ital., 75, 158
Borkova T. V., Marsakov V. A., 2005, Astron. Rep., 49, 405
Cardiel N., 1999, Ph.D. thesis, Universidad Complutense de Madrid, Spain
Carney B. W., Latham D. W., Laird J. B., Aguilar L. A., 1994, AJ, 107, 2240
Cenarro A. J. et al., 2007, MNRAS, 374, 664 (C07)
Chavez M., Malagnini M. L., Morossi C., 1997, A&AS, 126, 267
Chen Y.-P., Trager S. C., Peletier R. F., Lançon A., Vazdekis A., Prugniel P., Silva D. R., Gonneau A., 2014, A&A, 565, A117
Coelho P., Barbuy B., Meléndez J., Schiavon R. P., Castilho B. V., 2005, A&A, 443, 735
Conroy C., Graves G. J., van Dokkum P. G., 2014, ApJ, 780, 33
Cunha K. et al., 2015, ApJ, 798, L41
Dias W. S., Alessi B. S., Moitinho A., Lépine J. R. D., 2002, A&A, 389, 871
Donor J. et al., 2018, AJ, 156, 142
Dyck H. M., Benson J. A., van Belle G. T., Ridgway S. T., 1996, AJ, 111, 1705
Edvardsson B., Andersen J., Gustafsson B., Lambert D. L., Nissen P. E., Tomkin J., 1993, A&AS, 102, 603
Falcón-Barroso J., Sánchez-Blázquez P., Vazdekis A., Ricciardelli E., Cardiel N., Cenarro A. J., Gorgas J., Peletier R. F., 2011, A&A, 532, A95
Fitzpatrick E. L., 1999, PASP, 111, 63
Friedemann C., 1992, Bull. Inf. Cent. Donnees Stellaires, 40, 31
García Pérez A. E. et al., 2016, AJ, 151, 144
Gonneau A. et al., 2020, A&A, 634, A133
Gorgas J., Faber S. M., Burstein D., Gonzalez J. J., Courteau S., Prosser C., 1993, ApJS, 86, 153
Harris W. E., 1996, AJ, 112, 1487
Husser T.-O., Wende-von Berg S., Dreizler S., Homeier D., Reiners A., Barman T., Hauschildt P. H., 2013, A&A, 553, A6
Irwin A. W., 1981, ApJS, 45, 621
Jacobson H. R., Pilachowski C. A., Friel E. D., 2011, AJ, 142, 59
Jofré P. et al., 2018, Res. Notes. Am. Astron. Soc., 2, 152
Jones L. A., 1999, PhD thesis, Univ. of North Carolina
Kesseli A. Y., West A. A., Veyette M., Harrison B., Feldman D., Bochanski J. J., 2017, ApJS, 230, 16
Kipper T., Jorgensen U. G., 1994, A&A, 290, 148
Koesterke L., 2009, AIP Conf. Proc. Vol. 1171, Recent Directions in Astrophysical Quantitative Spectroscopy and Radiation Hydrodynamics. Am. Inst. Phys., New York, p. 73
Koesterke L., Allende Prieto C., Lambert D. L., 2008, ApJ, 680, 764
Koleva M., Prugniel P., Bouchard A., Wu Y., 2009, A&A, 501, 1269
Korn A. J. et al., 2007, ApJ, 671, 402
La Barbera F., Vazdekis A., Ferreras I., Pasquali A., Allende Prieto C., Röck B., Aguado D. S., Peletier R. F., 2017, MNRAS, 464, 3597
Le Borgne J.-F. et al., 2003, A&A, 402, 433
Lejeune T., Cuisinier F., Buser R., 1997, A&AS, 125, 229
Lejeune T., Cuisinier F., Buser R., 1998, A&AS, 130, 65
Mahdi D., Soubiran C., Blanco-Cuaresma S., Chemin L., 2016, A&A, 587, A131
Martins L. P., González Delgado R. M., Leitherer C., Cerviño M., Hauschildt P., 2005, MNRAS, 358, 49
Mermilliod J.-C., Mermilliod M., Hauck B., 1997, A&AS, 124, 349
Mészáros S., Allende Prieto C., 2013, MNRAS, 430, 3285
Mészáros S. et al., 2012, AJ, 144, 120
Mészáros S. et al., 2015, AJ, 149, 153
Milone A. D. C., Sansom A. E., Sánchez-Blázquez P., 2011, MNRAS, 414, 1227 (MSS11)
Mishenina T. V., Soubiran C., Kovtyukh V. V., Korotin S. A., 2004, A&A, 418, 551
Nelder J. A., Mead R., 1965, Comput. J., 7, 308
Nissen P. E., Schuster W. J., 2010, A&A, 511, 10
Pickles A. J., 1998, PASP, 110, 863
Press W. H., Flannery B. P., Teukolsky S. A., 1986, Numerical Recipes. The Art of Scientific Computing. Cambridge Univ. Press, Cambridge
Prugniel P., Soubiran C., 2001, A&A, 369, 1048
Prugniel P., Vauglin I., Koleva M., 2011, A&A, 531, A165
Ramírez S. V., Cohen J. G., Buss J., Briley M. M., 2001, AJ, 122, 1429
Sánchez-Blázquez P. et al., 2006, MNRAS, 371, 703
Savage B. D., Massa D., Meade M., Wesselius P. R., 1985, ApJS, 59, 397
Schuster W. J., Nissen P. E., Parrao L., Beers T. C., Overgaard L. P., 1996, A&AS, 117, 317
Schwenke D. W., 1998, Faraday Discuss., 109, 321
Sharma K., Prugniel P., Singh H. P., 2016, A&A, 585, A64
Silva D. R., Cornell M. E., 1992, ApJS, 81, 865
Snow T. P., Lamers H. J. G. L. M., Lindholm D. M., Odell A. P., 1994, ApJS, 95, 163
Soubiran C., Triaud A., 2004, A&A, 418, 1089
Soubiran C., Katz D., Cayrel R., 1998, A&AS, 133, 221
Soubiran C., Le Campion J.-F., Cayrel de Strobel G., Caillo A., 2010, A&A, 515, A111
Souto D. et al., 2018, ApJ, 857, 14
Stephens A., Boesgaard A. M., 2002, AJ, 123, 1647
Stetson P. B., Bruntt H., Grundahl F., 2003, PASP, 115, 413
Taylor B. J., 1999, A&AS, 134, 523
Thevenin F., 1998, Pub. VizieR On-line Data Catalog: III/193
Twarog B. A., Ashman K. M., Anthony-Twarog B. J., 1997, AJ, 114, 2556
Valdes F., Gupta R., Rose J. A., Singh H. P., Bell D. J., 2004, ApJS, 152, 251
Vazdekis A., Cenarro A. J., Gorgas J., Cardiel N., Peletier R. F., 2003, MNRAS, 340, 1317
Vazdekis A., Sánchez-Blázquez P., Falcón-Barroso J., Cenarro A. J., Beasley M. A., Cardiel N., Gorgas J., Peletier R. F., 2010, MNRAS, 404, 1639
Vazdekis A. et al., 2015, MNRAS, 449, 1177
Westera P., Lejeune T., Buser R., Cuisinier F., Bruzual G., 2002, A&A, 381, 524
Worthey G., Faber S. M., Gonzalez J. J., Burstein D., 1994, ApJS, 94, 687
Xiang M. S. et al., 2015, MNRAS, 448, 822
Yan R., MaStar Team, 2017, in Coelho P., Martins L., Griffin E., eds, ASI Con. Ser., Vol. 14, Spectral Stellar Libraries. p. 99

## SUPPORTING INFORMATION

Supplementary data are available at *MNRAS* online.

**Table 6.** Photospheric parameters and abundances estimates for field stars in MILES accompanied by their associated FERRE uncertainties, a flag describing the quality of the parameters (see Section 4), and the MILES numeric identification.
**Table 8.** Photospheric parameters and abundance estimates of cluster stars accompanied by their associated FERRE uncertainties, a flag describing the quality of the estimates (see Section 4), and the MILES numeric identification.
**Table 10.** Photospheric parameters and abundance estimates of the extra sample accompanied by their associated FERRE uncertainties and a flag describing the quality of the estimates (see Section 4).

Please note: Oxford University Press is not responsible for the content or functionality of any supporting materials supplied by the authors. Any queries (other than missing material) should be directed to the corresponding author for the article.

## APPENDIX: THE BLUE END OF THE SPECTRAL RANGE IN RUN A

The second-order filter used in the first run blocked wavelengths shorter than ∼3900 Å. Therefore, stars observed during this run do not have information in the blue end of the spectral range. For these stars, an extension of the observed spectra to bluer wavelengths down to ∼3540 Å is made adopting the interpolation algorithm described in Vazdekis et al. (2003), as updated in Vazdekis et al. (2015) to incorporate the Mg/Fe abundance parameter. The interpolation is done over the MILES spectra that cover the full wavelength range and uses the stellar parameters presented in this study. Fig. A1 illustrates this correction by comparing the spectrum of a star (HD 99233) observed in run A with the full spectrum of a star (HD 222493) observed in run B. The flux at wavelengths blueward of 3900 Å, obtained from interpolation, is also shown.

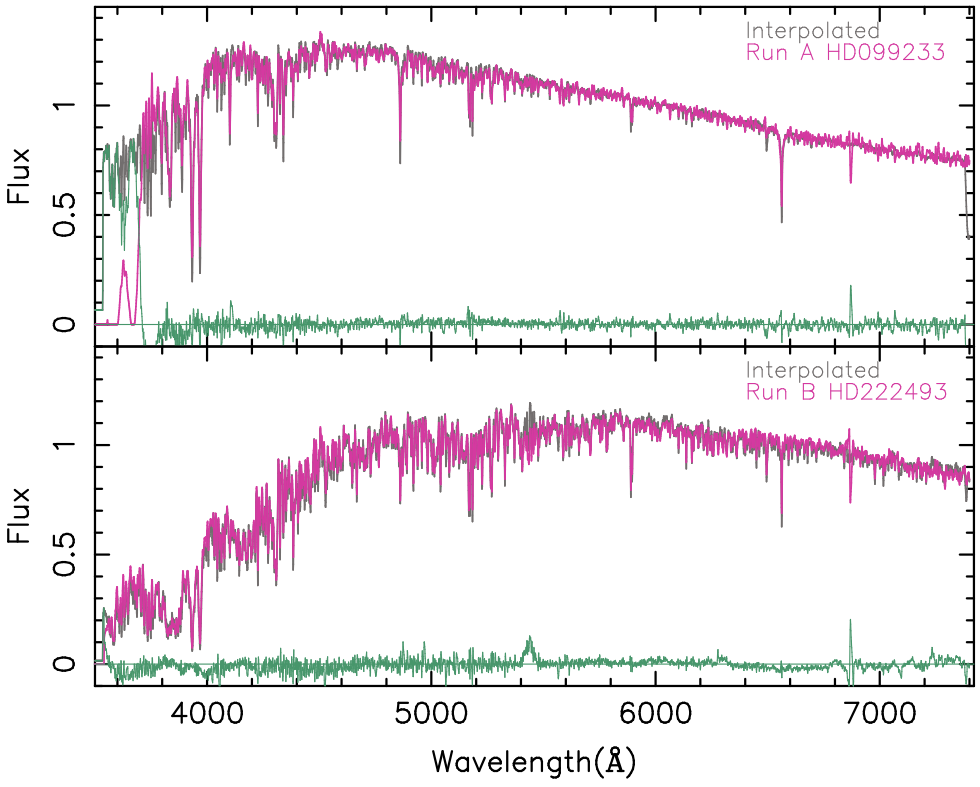


**Figure A1.** Top panel: Comparison of the full spectrum of the star HD 99233 observed in the first run (magenta) with an interpolated spectrum with the same atmospheric parameters (black). There is no observed signal for $\lambda \lesssim 3900$ Å because of the use of a second-order filter that blocked these wavelengths. Residuals (differences between reduced and interpolated spectra) are shown in green. Bottom panel: Same comparison but for the star HD 222493, which was observed in the second run.

This paper has been typeset from a TEX/LATEX file prepared by the author.